Physics of Fluids ARTICLE scitation.org/journal/phf

Capillary condensation of saturated vapor in a corner formed by two intersecting walls

Cite as: Phys. Fluids **34**, 062103 (2022); doi: 10.1063/5.0095845
Submitted: 13 April 2022 · Accepted: 17 May 2022 ·
Published Online: 1 June 2022

View Online Export Citation CrossMark

E. S. Benilov[a]

AFFILIATIONS

Department of Mathematics and Statistics, University of Limerick, Limerick V94 T9PX, Ireland

[a]Author to whom correspondence should be addressed: Eugene.Benilov@ul.ie. URL: https://staff.ul.ie/eugenebenilov/

ABSTRACT

The dynamics of saturated vapor between two intersecting walls is examined. It is shown that, if the angle ϕ between the walls is sufficiently small, the vapor becomes unstable, and spontaneous condensation occurs in the corner, similar to the so-called capillary condensation of vapor into a porous medium. As a result, an ever-growing liquid meniscus develops near the corner. The diffuse-interface model and the lubrication approximation are used to demonstrate that the meniscus grows if and only if $\phi + 2\theta < \pi$, where θ is the contact angle corresponding to the fluid/solid combination under consideration. This criterion has a simple physical explanation: if it holds, the meniscus surface is concave—hence, the Kelvin effect causes condensation. Once the thickness of the condensate exceeds by an order of magnitude the characteristic interfacial thickness, the volume of the meniscus starts to grow linearly with time. If the near-vertex region of the corner is smoothed, the instability can be triggered off only by finite-size perturbations, such that it includes enough liquid to cover the smoothed area by a microscopically thin liquid film.

I. INTRODUCTION

Saturated vapor and liquid are supposed to be in equilibrium—thus, if a small amount of the latter is placed in a container filled with the former, no exchange of mass should occur.

This simple conclusion—no matter how natural—is misleading: if the liquid is placed in a sufficiently acute (or not too obtuse) corner, mass exchange does occur. This result is obtained in the present paper for a narrow range of parameters, using an elaborate mathematical model—but it has a simple qualitative explanation and, thus, is likely to hold generally.

Consider a small meniscus in a corner formed by two walls intersecting at an angle ϕ (see Fig. 1) and introduce the microscopic contact angle θ at which the meniscus free boundary approaches the walls. Theoretically, θ is specific to the fluid/substrate combination under consideration (e.g., Ref. 1), but in reality the walls are never perfectly flat and chemically homogeneous. Microscopic imperfections give rise to a hysteresis interval, i.e., a certain spread in θ (e.g., Ref. 2); in what follows, it is assumed narrow—hence, insignificant—and is neglected.

Now, let ϕ and θ be such that

$$\phi + 2\theta < \pi, \tag{1}$$

in which case the free surface of the meniscus is concave (see Fig. 1). As a result, the Kelvin effect[3–10] gives rise to a vapor-to-liquid mass flux, making the meniscus absorb fluid from the surrounding vapor and grow—in a manner, similar to the effect of capillary condensation of vapor into a porous medium (e.g., Ref. 11). If, on the other hand, condition (1) does not hold, the surface of the meniscus is convex, and the Kelvin effect makes it dry up. This explains physically the nonexistence of solutions describing static liquid ridges[12] and three-dimensional drops[13]—in both cases, on a flat substrate and surrounded by saturated vapor.

The two possible behaviors of menisci could be described using the classical Navier–Stokes equations, coupled to a model of vapor diffusion in the surrounding air, with a boundary condition describing condensation and/or evaporation at the interface (e.g., Refs. 3–8, 10, and 14–19). Alternatively (as done in the present paper), the problem can be examined using the diffuse-interface model (DIM): it includes both hydro- and thermodynamics and, thus, consistently describes all of the effects arising in the problem at hand.

The diffuse-interface model (DIM) was invented as a tool for modeling interfaces based on two assumptions put forward by Ref. 20 in application to equilibrium interfaces in fluids:

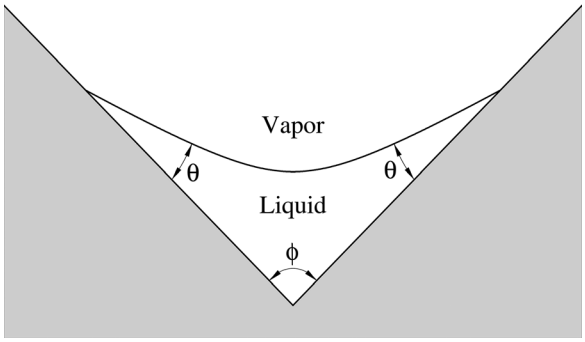

FIG. 1. A liquid meniscus in a corner (the region occupied by the solid is shaded). In the configuration shown, the contact angle θ is such that $\phi + 2\theta < \pi$, so spontaneous condensation occurs.

1. the van der Waals intermolecular force (responsible for phase transitions) can be described by a pair-wise potential,
2. the characteristic length of this potential is much smaller than the interfacial thickness.

In recent times, the DIM was incorporated into non-equilibrium fluid dynamics (see Refs. 21 and 22 and references therein) and applied to numerous problems including nucleation and collapse of bubbles,[23–26] phase separation in polymer blends,[27,28] contact lines,[29,30] contact lines in fluids with surfactants,[31,32] Faraday instability,[33,34] Rayleigh–Taylor instability,[35] etc. The DIM was shown to follow from the Enskog–Vlasov kinetic theory[36,37]—the same way the usual compressible hydrodynamics follows from Enskog's theory of dense fluids.[38] The DIM as a single equation applicable, under certain conditions, to all systems with phase transitions and interfaces was formulated in Ref. 39. An incompressible version of the DIM was formulated in Ref. 40 and applied to various problems involving contact lines (e.g., Refs. 41–44).

The DIM has been used for modeling settings involving the Kelvin effect. It was argued in Refs. 12 and 13 that two- and three-dimensional sessile drops cannot be static due to the Kelvin-effect-induced evaporation. The dynamics of a spherical drop floating in under- or oversaturated vapor of the same fluid was examined in Ref. 45: it was shown that the evaporation in this case is caused by advection of vapor by an outward flow due to a weak imbalance between the chemical potentials of the liquid and vapor. In mixtures, this mechanism acts alongside the diffusion (say, of vapor in air examined in Refs. 3–8, 10, and 14–19)—but in pure fluids (which do not diffuse), it is the *only* mechanism of evaporation. This makes the DIM an excellent tool for studying phase transitions in pure fluids.

The present paper applies the original (compressible) version of the DIM to a pure fluid bounded by two intersecting walls, under an additional assumption that the angle between the walls is almost straight ($\phi \approx \pi$) and they are made of a hydrophilic material ($\theta \ll 1$). This way, one can simplify the problem through the lubrication approximation—and even more so, since the lubrication approximation for a flat substrate ($\phi = \pi$) is already in place,[46] as is a framework for estimating the DIM parameters for a specific fluid.[47]

In Sec. II of the present paper, the problem will be formulated mathematically. Sections III and IV examine solutions describing static and evolving menisci, respectively. The lubrication approximation of the DIM is derived in Appendix B and summarized in Sec. V in a self-contained form that can be used for modeling thin drops with moving contact lines. Section V also provides an estimate of the dimensional timescale of capillary condensation of liquid films for a real-life example.

II. FORMULATION

A. Thermodynamics

The thermodynamic properties of a fluid can be described by the dependence of its internal energy e and entropy s (both specific, or per unit mass) on the density ρ and temperature T.[48] The functions $e(\rho, t)$ and $s(\rho, t)$ are not fully arbitrary as they should satisfy the fundamental thermodynamic (Gibbs) relation, which can be written in the form

$$\frac{\partial e}{\partial T} = T\frac{\partial s}{\partial T}. \tag{2}$$

Then, the equation of state (the expression for the pressure p as a function of ρ and T) is given by

$$p = \rho^2\left(\frac{\partial e}{\partial \rho} - T\frac{\partial s}{\partial \rho}\right), \tag{3}$$

and the specific chemical potential, or Gibbs free energy, by

$$G = e - Ts + \frac{p}{\rho}. \tag{4}$$

It follows from (2)–(4) that

$$\frac{\partial p}{\partial \rho} = \rho\frac{\partial G}{\partial \rho}, \tag{5}$$

$$\frac{\partial p}{\partial T} = \rho\left(\frac{\partial G}{\partial T} + s\right), \tag{6}$$

$$\frac{\partial G}{\partial T} = -\frac{\partial(\rho s)}{\partial \rho}. \tag{7}$$

These identities will be needed later, as well as the definition of the parameter,

$$B = p - \rho^2\frac{\partial e}{\partial \rho}.$$

$B(\rho, T)$ is not one of the standard thermodynamic functions, but it is convenient when thermodynamics is coupled to fluid dynamics. It characterizes the production/consumption of thermal energy due to mechanical compression/expansion of the fluid (more details to follow). Using definition (3) of p, one can represent B in the form

$$B = -\rho^2 T\frac{\partial s}{\partial \rho}. \tag{8}$$

B. Governing equations

A flow of a non-ideal fluid can be characterized by the density ρ, temperature T, and velocity $\mathbf{v} = (u, v, w)$—depending on the spatial coordinates (x, y, z) and time t. Also assume that the fluid is affected by a bulk force $\mathbf{F}$, which will be later identified with the intermolecular attraction (sometimes referred to as the van der Waals attraction).

Using the identity

$$\frac{1}{\rho}\nabla p = s\nabla T + \nabla G$$

[which follows from (5) and (6)], one can write the standard hydrodynamic equations in the form

$$\frac{\partial \rho}{\partial t} + \nabla \cdot (\rho \mathbf{v}) = 0, \tag{9}$$

$$\frac{\partial \mathbf{v}}{\partial t} + (\mathbf{v}\cdot\nabla)\mathbf{v} + s\nabla T + \nabla G = \frac{1}{\rho}\nabla\cdot\Pi + \mathbf{F}, \tag{10}$$

$$\rho c\left(\frac{\partial T}{\partial t} + \mathbf{v}\cdot\nabla T\right) + B\nabla\cdot\mathbf{v} = \Pi : \nabla\mathbf{v} + \nabla\cdot(\kappa\nabla T), \tag{11}$$

where the dotless product of two vectors produces a second-order tensor, the symbol ":" denotes the double scalar product of such tensors,

$$\Pi = \mu_s\left[\nabla\mathbf{v} + (\nabla\mathbf{v})^T - \frac{2}{3}\mathbf{I}(\nabla\cdot\mathbf{v})\right] + \mu_b\,\mathbf{I}(\nabla\cdot\mathbf{v}) \tag{12}$$

is the viscous stress tensor, $\mathbf{I}$ is the identity matrix, μ_s (μ_b) is the shear (bulk) viscosity, κ is the thermal conductivity, and c is the heat capacity at constant volume (the traditionally used subscript $_V$ is omitted).

Note that μ_s, μ_b, κ, c, and B depend generally on ρ and T. Observe also that the term involving B in Eq. (11) describes the production or consumption of thermal energy due to the fluid's compression ($\nabla\cdot\mathbf{v} < 0$) or expansion ($\nabla\cdot\mathbf{v} > 0$), respectively.

The diffuse-interface model (DIM) assumes the following expression for the van der Waals force:

$$\mathbf{F} = K\nabla\nabla^2\rho, \tag{13}$$

where the Korteweg parameter K is a fluid-specific constant, not depending on ρ and T.

Equations (9)–(12) (with an unspecified force $\mathbf{F}$) have been derived by Ref. 38 from Enskog's theory of dense fluids. For numerous other derivations, through irreversible thermodynamics and similar models, see the references cited by Refs. 36 and 48. The full set (9)–(13), including the expression for $\mathbf{F}$, was derived in Ref. 36 from the Enskog–Vlasov kinetic equation.

C. Boundary conditions at the substrate

Assume that the fluid is bounded below by a solid substrate whose shape is given by $z = H(x, y)$—see Fig. 2. This implies the no-flow boundary condition,

$$\mathbf{v} = \mathbf{0} \quad \text{at} \quad z = H. \tag{14}$$

Let the substrate be kept at a fixed temperature,

$$T = T_0 \quad \text{at} \quad z = H. \tag{15}$$

Physically, this boundary condition implies that the substrate is sufficiently thick, and the heat conductivity of the material it is made of is sufficiently large—in which case it is able to "hold" its temperature regardless of the heat flux coming from the fluid. Also note that the results of this work are not sensitive to the choice of the boundary condition for the temperature, and so (15) could be replaced with, say, the condition of insulation (zero heat flux).

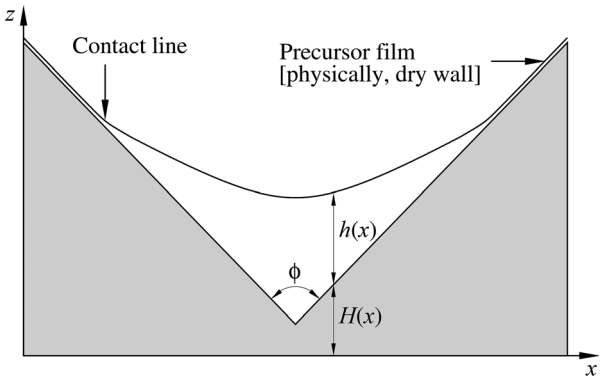

FIG. 2. Formulation of the problem.

Due to the presence of higher-order derivatives of ρ in expression (13) for the van der Waals force, an extra boundary condition is required for the density. There are several versions of such in the literature (e.g., Refs. 22 and 49), of which the simplest one is used in this work,

$$\rho = \rho_0 \quad \text{at} \quad z = H, \tag{16}$$

where ρ_0 is a phenomenological parameter. The physical meaning of this condition can be clarified by considering the van der Waals force acting on the fluid in the near-substrate boundary layer: the solid attracts it *toward* the substrate, while the fluid outside the boundary layer pulls it *away* from the substrate. The former force is fixed, whereas the latter grows with the near-substrate density, so the balance is achieved when the density assumes a certain value—which is precisely what condition (16) prescribes.

In addition to the advantage of simplicity, condition (16) can be derived under the same assumptions as the DIM itself.[47] Furthermore, since the expected effect of spontaneous condensation depends only on the curvature of the meniscus interface (as argued in the Introduction), the model used for the boundary condition is not essential. Condensation occurs at the liquid/vapor interface, so the fluid/substrate interaction affects it weakly.

D. Boundary conditions far above the substrate

Assume that, far above the substrate, the tangential stress and vertical heat flux are both zero,

$$\frac{\partial \mathbf{v}}{\partial z} \to \mathbf{0} \quad \text{as} \quad z \to +\infty, \tag{17}$$

$$\frac{\partial T}{\partial z} \to 0 \quad \text{as} \quad z \to +\infty. \tag{18}$$

As explained in the Introduction, this paper is concerned with the dynamics of *saturated* vapor—thus, assume

$$\rho \to \rho_v \quad \text{as} \quad z \to +\infty. \tag{19}$$

The saturated vapor density ρ_v, together with the matching liquid density ρ_l, depends on the temperature and is determined by the so-called Maxwell construction,

$$G(\rho_v, T) = G(\rho_l, T), \tag{20}$$
$$p(\rho_v, T) = p(\rho_l, T). \tag{21}$$

One should also require that the vapor and liquid be thermodynamically stable, which amounts to

$$\left(\frac{\partial p}{\partial \rho}\right)_{\rho=\rho_v} \geq 0, \quad \left(\frac{\partial p}{\partial \rho}\right)_{\rho=\rho_l} \geq 0,$$

i.e., an increase in ρ should not reduce the pressure. Note that p in the above inequalities can be replaced with the chemical potential G as their derivatives with respect to ρ are of the same sign [see identity (5)]. An illustration of the Maxwell construction can be found in Fig. 3.

For realistic $G(\rho, T)$ and $p(\rho, T)$ and a sufficiently low (*subcritical*) temperature T, Eqs. (20) and (21) admit a unique solution for the pair (ρ_v, ρ_l) such that $\rho_v < \rho_l$. For a sufficiently high (*supercritical*) T, (20) and (21) can only be satisfied by the trivial solution $\rho_v = \rho_l$, which physically means that only one phase exists. Everywhere in this paper, the temperature is assumed to be subcritical.

Physically, the Maxwell construction ensures that a liquid/vapor interface is in equilibrium: the equalities of the chemical potential and pressure in the two phases guarantee the thermodynamic and mechanical equilibria, respectively. Mathematically, conditions (20) and (21) can be derived from the DIM (see below) or any other adequate model by adapting the governing equations for the static isothermal flat interface in an unbounded space.

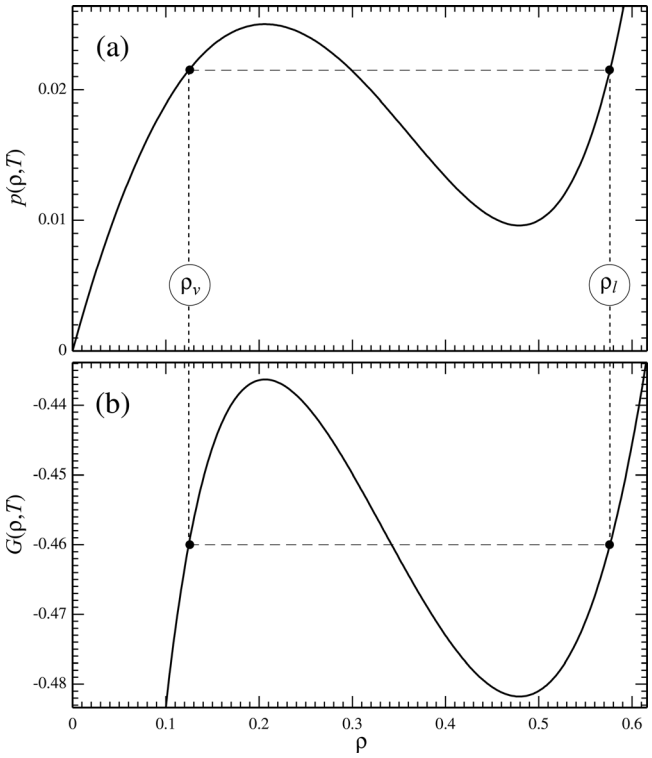

FIG. 3. An illustration of the Maxwell construction. Conditions (20) and (21) are illustrated in panels (b) and (a), respectively, for the particular case of the van der Waals fluid (42) and (43) with $T = 0.26$. Observe that $\partial p/\partial \rho$ and $\partial G/\partial \rho$ are positive at both $\rho = \rho_l$ and $\rho = \rho_v$ (so that the liquid and vapor phases are thermodynamically stable).

Let the near-substrate density prescribed by boundary condition (16) be such that

$$\rho_v < \rho_0 < \rho_l. \tag{22}$$

If this condition does not hold, the substrate becomes either perfectly hydrophobic ($\rho_0 \leq \rho_v$) or perfectly hydrophilic ($\rho_0 \geq \rho_l$).[22,47] In the former case, condensation cannot occur on the substrate (because it repulses the liquid phase), whereas the latter implies immediate condensation regardless of all other parameters.

E. How can liquid and vapor be distinguished in a continuous density field?

Since the DIM assumes the density to vary continuously (as opposed to being restricted to $\rho = \rho_v$ or $\rho = \rho_l$), one needs a formal definition of the position of the interface between the phases. The simplest option is to assume that the fluid with $\rho > \frac{1}{2}(\rho_v + \rho_l)$ should be treated as liquid and *vice versa*.

Thus, the liquid/vapor interface is defined to be located at the height $z = H + h$, where $h(x, y, t)$ is such that

$$\rho(x, y, H + h, t) = \frac{1}{2}(\rho_v + \rho_l). \tag{23}$$

To ensure that $h > 0$, one should require [in addition to restriction (22)] that

$$\rho_0 > \frac{1}{2}(\rho_v + \rho_l).$$

Given this condition, a layer exists adjacent to the substrate, $H < z < H + h$, which should be mathematically treated as liquid. Most importantly, even if one considers a horizontally localized drop or meniscus, this layer stretches to infinity in all horizontal directions (see a schematic in Fig. 2)—which was probably what prompted[22] to dub it a "precursor film." Yet, physically, it corresponds to dry substrate—or, equivalently, to the solid/vapor interface.

Let $\bar{h}$ be the thickness of the precursor film on a flat unbounded substrate; as shown below, $\bar{h}$ depends on the fluid's thermodynamic properties and the Korteweg parameter K. One should keep in mind that, by comparison with typical sizes of capillary menisci (ranging from 0.1 mm to 1 cm), $\bar{h}$ is miniscule (on a nanoscale). In what follows, such scales will be referred to as "microscopic."

III. STATIC MENISCI

A. Nondimensionalization

Let the fluid be at rest, $\mathbf{v} = \mathbf{0}$, which also implies steadiness of the density field, $\partial \rho/\partial t = 0$, and isothermality, $T = T_0$ (otherwise the heat flux would generate a flow). With this in mind, and considering for simplicity the two-dimensional (2D) case, one can reduce (9)–(13) to a single equation for $\rho(x, y)$,

$$K\left(\frac{\partial^2 \rho}{\partial x^2} + \frac{\partial^2 \rho}{\partial z^2}\right) - G(\rho, T) + G(\rho_v, T) = 0, \tag{24}$$

where T_0 was re-denoted $T_0 \to T$ and the value of the constant of integration (the last term on the left-hand side) was deduced from

boundary condition (19). Physically, this (elliptic nonlinear) equation describes the balance of the van der Waals force and pressure gradient. For an illustration of the nonlinearity present in Eq. (24) (via the dependence of G on ρ), the reader is referred to Fig. 3(b).

To nondimensionalize Eq. (24), introduce a characteristic density ϱ, pressure P, and the interfacial thickness,

$$l = \sqrt{\frac{K\varrho^2}{P}}. \tag{25}$$

Estimates show that l is on a nanometer scale.[24,26,47]

As shown by Ref. 22, the vertical-to-horizontal aspect ratio of a liquid film can be identified with

$$\varepsilon = \frac{\rho_l - \rho_0}{\rho_l}.$$

Thus, a meniscus can be regarded thin only if the near-wall density ρ_0 is close to the liquid density ρ_l.

The following nondimensional variables will be used:

$$x_{nd} = \frac{x}{\varepsilon^{-1} l}, \quad z_{nd} = \frac{z}{l}, \quad H_{nd} = \frac{H}{l}, \tag{26}$$

$$\rho_{nd} = \frac{\rho}{\varrho}, \quad T_{nd} = \frac{\varrho R T}{P}, \tag{27}$$

$$p_{nd} = \frac{p}{P}, \quad G_{nd} = \frac{\varrho G}{P}, \tag{28}$$

where R is the specific gas constant. Also introduce

$$(\rho_0)_{nd} = \frac{\rho_0}{\varrho}, \quad (\rho_v)_{nd} = \frac{\rho_v}{\varrho}, \quad (\rho_l)_{nd} = \frac{\rho_l}{\varrho}. \tag{29}$$

In terms of the new variables, Eq. (24) and boundary conditions (16) and (19) take the form (the subscript $_{nd}$ omitted),

$$\varepsilon^2 \frac{\partial^2 \rho}{\partial x^2} + \frac{\partial^2 \rho}{\partial z^2} - G(\rho, T) + G(\rho_v, T) = 0, \tag{30}$$

$$\rho = \rho_l - \varepsilon \quad \text{at} \quad z = 0, \tag{31}$$

$$\rho \to \rho_v \quad \text{as} \quad z \to +\infty. \tag{32}$$

B. 1D solutions of Eq. (30)

First consider the solution $\bar{\rho}(z)$ of Eq. (30) that describes a flat liquid/vapor interface in an unbounded space (i.e., without a substrate). For this case, Eq. (30) and boundary condition (32) become

$$\frac{\mathrm{d}^2 \bar{\rho}}{\mathrm{d}z^2} - G(\bar{\rho}, T) + G(\rho_v, T) = 0, \tag{33}$$

$$\bar{\rho} \to \rho_v \quad \text{as} \quad z \to +\infty, \tag{34}$$

whereas the substrate boundary condition should be replaced with

$$\bar{\rho} \to \rho_l \quad \text{as} \quad z \to -\infty. \tag{35}$$

Due to the translational invariance of boundary-value problem (33)–(35), its solution is not unique. To make it such, require

$$\bar{\rho}(0) = \frac{1}{2}(\rho_l + \rho_v). \tag{36}$$

For a physically meaningful $G(\rho, T)$, $\bar{\rho}(z)$ is a kink-like function, decreasing monotonically with increasing z.

The boundary-value problem for $\bar{\rho}(z)$ can be used to derive the Maxwell construction. Its first "half"—equality (20)—can be derived by considering Eq. (33) in the limit $z \to -\infty$. Equality (21), in turn, can be obtained by multiplying (33) by $\mathrm{d}\bar{\rho}/\mathrm{d}z$ and integrating; taking into account identity (5) and fixing the constant of integration via boundary condition (34), one obtains

$$\frac{1}{2}\left(\frac{\mathrm{d}\bar{\rho}}{\mathrm{d}z}\right)^2 - \bar{\rho}[G(\bar{\rho}, T) - G(\rho_v, T)] + p(\bar{\rho}, T) - p(\rho_v, T) = 0. \tag{37}$$

Considering this equation in the limit $z \to -\infty$ and using the (already proven) equality (20), one can obtain (21) as required.

The solution $\bar{\rho}(z)$ of Eq. (37) subject to boundary condition (36) can be readily found in an implicit form,

$$\int_{\frac{1}{2}(\rho_l+\rho_v)}^{\bar{\rho}} \frac{2^{-1/2}\mathrm{d}\rho}{\sqrt{\rho[G(\rho, T) - G(\rho_v, T)] - p(\rho, T) + p(\rho_v, T)}} = -z. \tag{38}$$

Next, introduce a substrate and let it be flat ($H = \text{const}$). The solution describing this situation can be expressed in terms of the function $\bar{\rho}(z)$: shifting it to satisfy the boundary condition at the substrate, one obtains $\rho = \bar{\rho}(z - H - \bar{h})$ where $\bar{h}$ is such that

$$\bar{\rho}(-\bar{h}) = \rho_0. \tag{39}$$

Physically, $\rho = \bar{\rho}(z - H - \bar{h})$ describes the precursor film on a dry substrate located at $z = H$, and $\bar{h}$ is the film's nondimensional thickness. Substituting (38) into (39), one obtains

$$\bar{h} = \int_{\frac{1}{2}(\rho_l+\rho_v)}^{\rho_l-\varepsilon} \frac{2^{-1/2}\mathrm{d}\rho}{\sqrt{\rho[G(\rho, T) - G(\rho_v, T)] - p(\rho, T) + p(\rho_v, T)}}. \tag{40}$$

It can be shown (see Appendix A 1) that $\bar{h}$ is logarithmically large,

$$\bar{h} = \frac{\ln \varepsilon^{-1}}{C} + \mathcal{O}(1),$$

where

$$C = \left[\left(\frac{\partial G}{\partial \rho}\right)_{\rho=\rho_l}\right]^{1/2} \tag{41}$$

is real (because the liquid was assumed to be thermodynamically stable—hence, $(\partial G/\partial \rho)_{\rho=\rho_l} > 0$).

C. An example: The van der Waals fluid

For the van der Waals fluid, the internal energy and entropy (both nondimensional and specific) are

$$e(\rho, T) = cT - \rho, \quad s(\rho, T) = c \ln T - \ln \frac{\rho}{1 - \rho},$$

where the heat capacity c has been nondimensionalized by the specific gas constant R. The corresponding expressions for pressure (3) and chemical potential (4) are

$$p(\rho, T) = \frac{T\rho}{1-\rho} - \rho^2, \tag{42}$$

$$G(\rho, T) = T\left(\ln\frac{\rho}{1-\rho} + \frac{1}{1-\rho} + c - c\ln T\right) - 2\rho + T(1 + c - c\ln T). \tag{43}$$

The solution of the Maxwell construction (20) and (21) for this case is shown in Fig. 4(a) (note that the nondimensional critical temperature of the van der Waals fluid is $T_{cr} = 8/27$).

Note that, for many common fluids at room temperature, $T \lesssim 0.1$ (see Table I of Ref. 50 where T is denoted by τ). Thus, it is worthwhile to examine the solution of the Maxwell construction in the limit $T \to 0$. For the van der Waals fluid, it is[46]

$$\rho_l = \frac{1+\sqrt{1-4T}}{2} + \mathcal{O}(\mathrm{e}^{-1/T}), \tag{44}$$

$$\rho_v = \frac{1+\sqrt{1-4T}}{1-\sqrt{1-4T}}\mathrm{e}^{-1/T} + \mathcal{O}(T^{-1}\mathrm{e}^{-2/T}). \tag{45}$$

Expression (45) shows that, if T is small, the vapor density is *exponentially* small, and the same can be assumed for all physically meaningful equations of states, not only the van der Waals one.

For $T \ll 1$, one can deduce from boundary-value problem (33)–(36) that

$$\bar\rho(z) = \begin{cases} 1 + \mathcal{O}(T) & \text{if} \quad z \le -2^{-3/2}\pi, \\ \frac{1}{2}(1 - \sin 2^{1/2}z) + \mathcal{O}(T) & \text{if} \quad -2^{-3/2}\pi \le z \le 2^{-3/2}\pi, \\ 0 + \mathcal{O}(T) & \text{if} \quad z \ge 2^{-3/2}\pi. \end{cases} \tag{46}$$

D. Asymptotic description of static menisci

Consider a static configuration with the liquid phase confined to a layer adjacent to the substrate, forming a 2D meniscus (liquid film). This implies that, with increasing z, the density first grows from ρ_0 to approximately ρ_l, and then decreases toward ρ_v.

The asymptotic description of menisci with a small aspect ratio is based on the observation that the general equation (30) for $\rho(x, z)$ is asymptotically close to (much simpler) Eq. (33) for $\bar\rho(z)$. Since the difference between the two equations is small, one can assume

$$\rho(x, z) \approx \bar\rho(z - H - h), \tag{47}$$

where the undetermined function $h(x)$ is, physically, the distance between the substrate and fluid/vapor interface (see Fig. 2).

On the basis of assumption (47), the following asymptotic equation for $h(x)$ is derived in Appendix A:

$$\sigma\frac{\mathrm{d}^2(H+h)}{\mathrm{d}x^2} = f(h - \bar h), \tag{48}$$

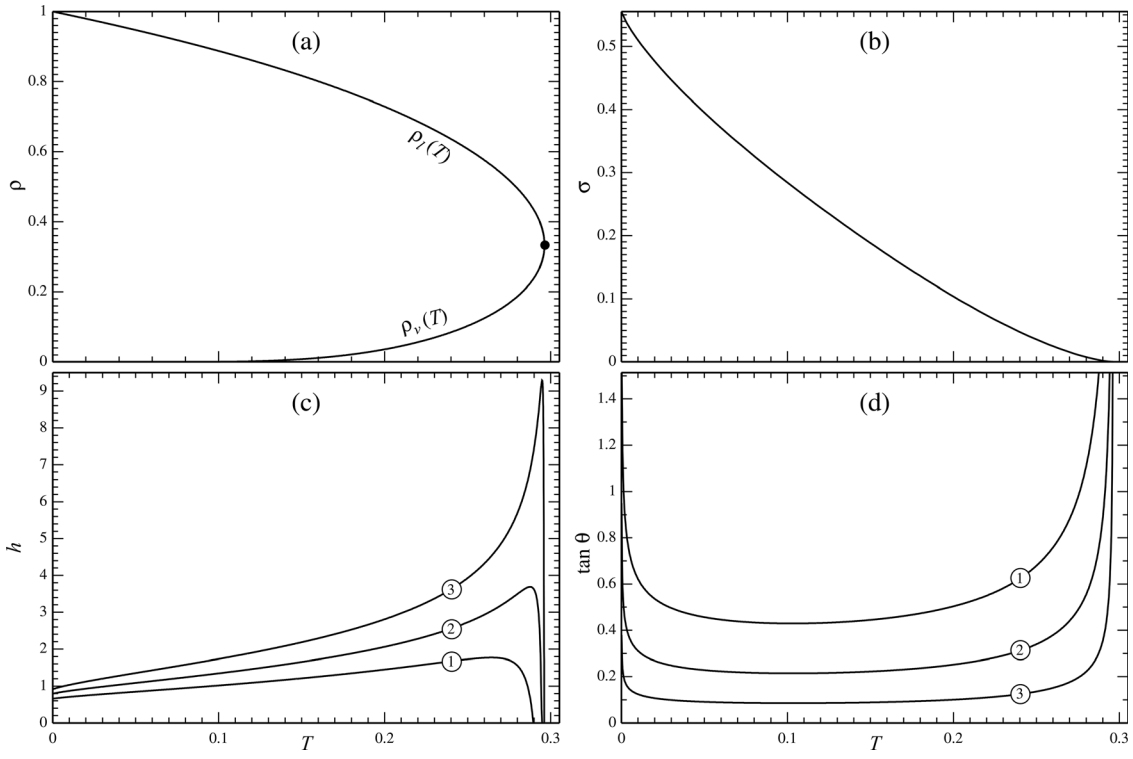

FIG. 4. Various characteristics of interfaces and contact lines vs the temperature: (a) densities of the liquid and vapor phases (the black dot marks the critical point); (b) surface tension; (c) precursor film's thickness; (d) tan θ, where θ is the contact angle. The curves in panels (c) and (d) correspond to (1) $\varepsilon = 0.1$; (2) $\varepsilon = 0.05$; and (3) $\varepsilon = 0.02$.

where

$$\sigma = \int_{-\infty}^{\infty} \left(\frac{\mathrm{d}\bar{\rho}}{\mathrm{d}z}\right)^2 \mathrm{d}z \tag{49}$$

is, physically, the surface tension, and the function

$$f(\xi) = 2C^2(1 - \mathrm{e}^{-C\xi})\mathrm{e}^{-C\xi}, \tag{50}$$

describes the effect exerted on the fluid by the substrate. Also recall that the precursor film thickness $\bar{h}$ is defined by (40) and coefficient C, by (41).

The coefficients $\sigma(T)$ and $\bar{h}(T, \varepsilon)$ have been computed for the van der Waals fluid [i.e., for G and p given by (42) and (43)] and are shown in Figs. 4(b) and 4(c), respectively. The former figure shows that the surface tension vanishes at the critical point (as it should). Note also that, since $\rho_v \to \rho_l$ as $T \to T_{cr}$ [as illustrated in Fig. 4(a)]—then, sooner or later, $\rho_0 = \rho_l - \varepsilon$ becomes smaller than ρ_v. This violates assumption (22) and also makes $\bar{h}$ negative, so this part of the graphs in Fig. 4(c) has been truncated.

Before considering menisci in a corner (which is the ultimate goal of this paper), it is instructive to examine the solution of Eq. (48) for a flat substrate with the following boundary condition:

$$h \to \bar{h} \quad \text{as} \quad x \to +\infty. \tag{51}$$

Substituting $H = \text{const}$ into Eq. (48), multiplying it by $\mathrm{d}h/\mathrm{d}z$, integrating with respect to z, and fixing the constant of integration via condition (51), one can obtain a separable equation. Its solution will be presented in a form that is best suited for physical interpretation,

$$h = \bar{h} + \frac{1}{C}\ln\left[1 + \exp\frac{C(x_0 - x)\tan\theta}{\varepsilon}\right], \tag{52}$$

where x_0 is arbitrary and θ is, at this stage, a constant such that

$$\tan\theta = \left(\frac{2C}{\sigma}\right)^{1/2}\varepsilon. \tag{53}$$

The physical meaning of θ can be deduced from the asymptotics of solution (52) at minus-infinity,

$$h \to -\frac{x}{\varepsilon}\tan\theta \quad \text{as} \quad x \to -\infty,$$

which describes a liquid/vapor interface inclined at an angle θ [the factor of $1/\varepsilon$ accounts for the different scalings of x and z in nondimensionalization (26)]. Thus, θ is the contact angle.

The dependence of θ on T, computed for the van der Waals fluid (42) and (43), is shown in Fig. 4(d). Observe that $\tan\theta \to \infty$ in both small-temperature and near-critical limits (which can also be deduced analytically from the asymptotic behavior of C and σ as $T \to 0$ and $T \to T_{cr}$). As a result, the lubrication approximation fails in these limits, and so the results of this paper are not applicable.

Examples of solution (52), computed for the van der Waals fluid and various temperatures, are shown in Fig. 5. Observe that the interfaces for $T = 0.05$ and $T = 0.15$ are almost parallel, which is a result of the near-constancy of θ in the middle part of Fig. 4(d).

E. Static menisci in a corner

Let the substrate form a corner of angle ϕ (as in Fig. 2), so that the substrate is described by

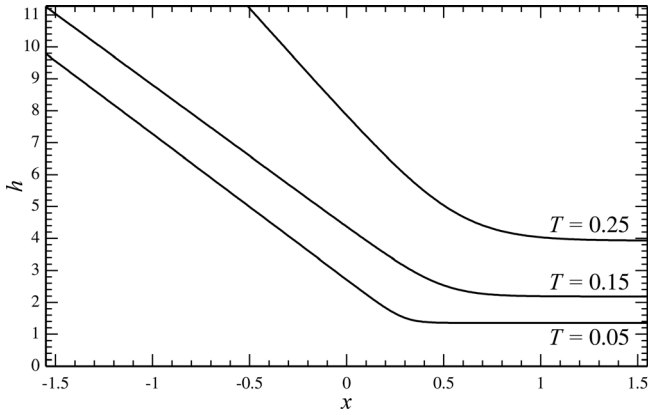

FIG. 5. Examples of solution (52) for $\varepsilon = 0.02$ and three values of the temperature (indicated in the figure).

$$H = \frac{|x|}{\varepsilon}\tan\frac{\pi - \phi}{2}. \tag{54}$$

Since the lubrication approximation used in this paper implies that $\theta \ll 1$ and $\phi \approx \pi$, "tan" can be omitted in (53) and (54), but it can be just as well kept (so that the results obtained would look more natural).

Given the substrate's symmetry, the meniscus surface should also be symmetric, which corresponds to the following boundary condition:

$$\frac{\mathrm{d}(H + h)}{\mathrm{d}x} = 0 \quad \text{at} \quad x = 0. \tag{55}$$

Assume also that, far from the corner, the substrate is dry, which implies

$$h \to \bar{h} \quad \text{as} \quad x \to \pm\infty.$$

Since, in the problem at hand,

$$\frac{\mathrm{d}^2 H}{\mathrm{d}x^2} = 0 \quad \text{if} \quad x \neq 0,$$

the general equation (48) reduces for $x \neq 0$ to that for a *flat* substrate. Using, thus, the same approach, one obtains

$$h = \bar{h} + \frac{1}{C}\ln\left[1 - \frac{\tan\frac{1}{2}(\pi - \phi)}{\tan\frac{1}{2}(\pi - \phi) - \tan\theta}\exp\left(-\frac{C|x|\tan\theta}{\varepsilon}\right)\right]. \tag{56}$$

Evidently, h is real—hence, physically meaningful—only if

$$\frac{1}{2}(\pi - \phi) \leq \theta. \tag{57}$$

Not surprisingly, this condition (of existence of static menisci) is the opposite of condition (1) of condensation.

Another restriction on the applicability of solution (56) originates from the requirement that h be non-negative—hence,

$$\tan\frac{1}{2}(\pi-\phi)\geq-\left(e^{C\bar{h}}-1\right)\tan\theta. \tag{58}$$

Observe that this condition can fail only if $\phi > 180°$.

Examples of static menisci described by solution (56) are shown in Fig. 6(a). They are all computed for the angle ϕ such that the existence condition (57) holds everywhere except a narrow interval,

$$0.102\,7 \lesssim T \lesssim 0.103\,3.$$

Evidently, when T approaches this interval, the core (middle part) of the meniscus becomes increasingly thick. This does not violate the lubrication approximation, however, as the slope of the interface remains small.

As for condition (58), it can be violated—at least, for the van der Waals fluid—only if T is very near its critical value and ϕ is near 2π. These requirements cut out a miniscule part of the problem's parameter space, not to mention that $\tan\theta$ is not small there—hence, the lubrication approximation fails. This effectively means that restriction (58) can be ignored.

Note, however, that substrates with a *sharp* corner—such as the one given by (54)—violate the lubrication approximation. One can still argue that the corner can be smoothed by an arc with a radius of curvature much larger than the thickness of the meniscus, but much smaller than the meniscus's width. In this case, the lubrication approximation holds, yet the solutions should be asymptotically close to that for the sharp corner.

It turns out, however, that smoothing of the corner changes the nature of the vapor instability, making this case worth studying. The general tendency will be illustrated by the following example of the substrate's shape:

$$H=\sqrt{\left(\frac{x}{\varepsilon}\tan\frac{\pi-\phi}{2}\right)^2+H_0^2e^{-(x/\Delta_H)^2}}, \tag{59}$$

where the constants H_0 and Δ_H determine the amplitude and width of smoothing, respectively. In this case, Eq. (48) cannot be solved analytically, but its solution can be readily found using the MATLAB function BVP4c (based on the three-stage Lobatto IIIa formula, see Ref. 51).

Typical results are shown in Fig. 6(b). Comparing it with 6(a), one might think that the smoothing reduces the size of the meniscus—which is true, but applies mostly to near-critical menisci (such that $\phi+2\theta\approx\pi$). This occurs because the smoothing expands their existence region beyond the restriction $\phi+2\theta\geq\pi$, and so near-critical menisci for a sharp corner are "far-from-critical" for the smoothed one.

Consider, for example, the smoothed corner described by Eq. (59) with

$$H_0=0.3,\quad \Delta=1, \tag{60}$$

in which case numerical computations suggest that menisci exist if

$$\tan\frac{1}{2}(\pi-\phi)\lesssim 0.087\,2.$$

For a sharp corner, in turn, the existence condition is given by restriction (1) which amounts to

$$\tan\frac{1}{2}(\pi-\phi)\leq\tan\theta\approx 0.085\,9.$$

The difference between the two existence criteria would be too slight to be important, should it not seem to invalidate the suggested physical interpretation of the main result of this paper, condition (1). If condensation does not occur in a situation where (1) holds, does this mean that concave menisci do not absorb moisture?

To resolve the apparent paradox, observe that a sufficiently small drop can have its contact lines in the *smoothed region* and, thus, not be sensitive to the global angle ϕ—as a result, it could be static. On the other hand, a sufficiently large drop with contact lines on the *flat* parts of the walls should still be unstable.

Mathematically, the existence of a static meniscus—even a stable one with respect to infinitesimal perturbation—does not necessarily

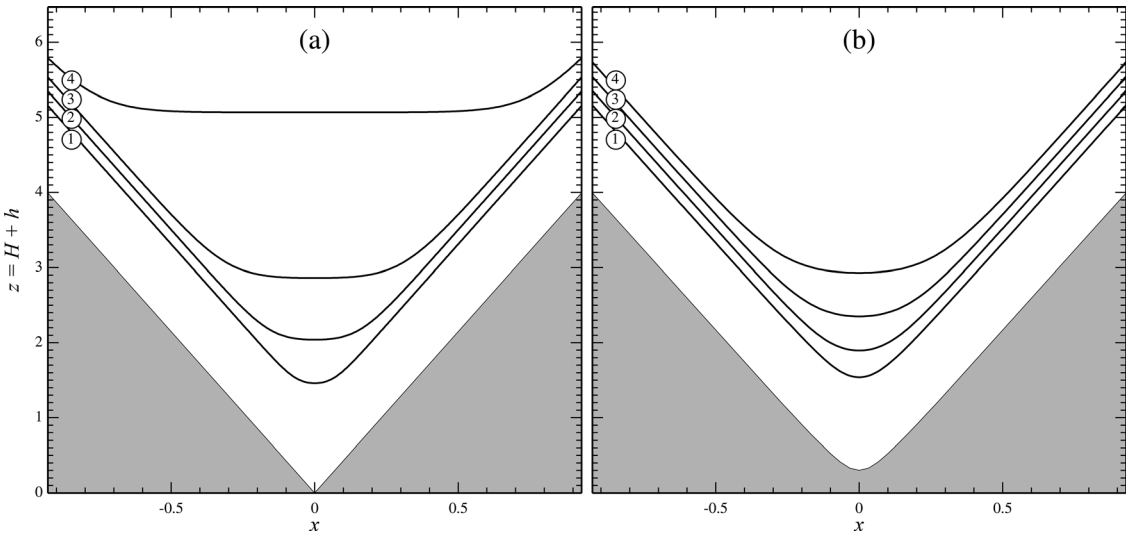

FIG. 6. Examples of static menisci with $\varepsilon = 0.02$, in a corner with $\tan\frac{1}{2}(\pi-\phi) = 0.085\,875$. Curves (1)–(4) correspond to $T = 0.025, 0.05, 0.075, 0.1$. (a) Solution (56) for the sharp corner. (b) The numerical solution for the smooth corner described by expressions (59) and (60).

mean the vapor is stable with respect to *finite-amplitude* perturbations. This issue will be clarified in Sec. IV by exploring the meniscus evolution.

IV. EVOLVING MENISCI

As shown Sec. III, steady menisci in a sharp corner exist only subject to condition (57), but it remains unclear what happens if (57) does not hold. One can only assume that menisci evolve in this case.

To find out how exactly they evolve, two evolution equations, corresponding to two asymptotic regimes, have been derived: regime 1 is applicable when $\rho_v \sim \rho_l$ (see Appendix B 1) and regime 2, when $\rho_v \ll \rho_l$ (Appendix B 2). According to the former, the dynamics is dominated by expansion (compression) of the fluid while it evaporates (condensates)—whereas, in the latter, these effects are as strong as advection by horizontal velocity. Motion-induced variations of temperature are small in both cases, but they can be neglected only in the latter regime (in the former, they still affect the leading-order dynamics). Most importantly, regime 2 applies to many common fluids at room temperature[50]—and, thus, will be discussed in detail; regime-1 solutions are qualitatively similar and, thus, will not.

Regime 2 ($\rho_v \ll \rho_l$) is governed by the following equation:

$$\frac{\partial h}{\partial t}+\frac{\partial}{\partial x}\left\{Q(h)\frac{\partial}{\partial x}\left[\sigma\frac{\partial^2(H+h)}{\partial x^2}-f(h-\bar{h})\right]\right\}=\frac{1}{\varepsilon^2 A}\left[\sigma\frac{\partial^2(H+h)}{\partial x^2}-f(h-\bar{h})\right]. \tag{61}$$

Here, the function f is defined by (50) and the rest of the coefficients are

$$A=0.142\,19\left[\mu_{b.v}(T)+\frac{4}{3}\mu_{s.v}(T)\right]\rho_l^2\rho_v^{-5/2}T^{1/2}, \tag{62}$$

$$Q(h)=\frac{1}{\rho_l^2}\int_0^\infty\frac{\hat{\rho}^2(z-h)}{\mu_s(\bar{\rho}(z-h),T)}\mathrm{d}z, \tag{63}$$

where $\mu_{s.v}(T)=\mu_s(\rho_v,T)$ and $\mu_{b.v}(T)=\mu_b(\rho_v,T)$ are the shear and bulk viscosities of the vapor, respectively, $\mu_s(\rho,T)$ is the fluid's shear viscosity in the whole density range, and

$$\hat{\rho}(z)=\int_z^\infty[\bar{\rho}(z')-\rho_v]\mathrm{d}z'. \tag{64}$$

To understand the physical meaning of Eq. (61), note that the two terms involving f describe how the substrate affects the liquid/vapor interface (since h is the distance between the two, it does not come as a surprise that $f\to 0$ as $h\to\infty$). Out of the two terms involving σ, the one on the left-hand side is the usual capillary term, whereas the one on the right-hand side describes either evaporation or condensation due to the Kelvin effect. Which among the two depends on the curvature of the liquid/vapor interface: if it is convex (concave), this term is negative (positive) and, thus, causes evaporation (condensation). Note also that, if $H=$ const, Eq. (61) coincides with its flat-substrate counterpart derived by Ref. 46.

To calculate the function $Q(h)$ [given by (63) and (64)], one needs to know the shear viscosity $\mu_s(\rho,T)$ and chemical potential $G(\rho,T)$ within the full density range $\rho_v<\rho<\rho_l$. In this paper, the simplest approximations are used for these parameters.

To qualitatively model the difference between the shear viscosity of vapor and that of liquid, it is assumed that

$$\mu_s=\rho, \tag{65}$$

where the coefficient of proportionality is implied to have been eliminated by letting the nondimensionalization scale μ be equal to the shear viscosity of the liquid phase. Such a choice also makes both $\mu_{s.v}$ and $\mu_{b.v}$ small.

As for $G(\rho,T)$, the van der Waals expression (43) was used, under the condition $T\ll 1$ (which ensures that $\rho_v\ll\rho_l$). In this case, $\bar{\rho}(z)$ is given by expression (46), and the liquid and vapor densities, by (44) and (45)—or, to leading order,

$$\rho_l=1,\quad \rho_v=0.$$

Substituting these equalities, together with (65) and (46), into expressions (63) and (64), and assuming that $h\geq 2^{-3/2}\pi\approx 1.110\,7$ (which is not restrictive, as h has already been assumed to be logarithmically large), one obtains

$$Q(h)=\frac{1}{3}h^3+2^{-5/2}\pi\left(1-\frac{\pi^2}{12}\right)\approx\frac{1}{3}h^3+0.098\,595. \tag{66}$$

For different $G(\rho,T)$ and $\mu_s(\rho,T)$, the numeric factor in the above formula would be different.

Equation (61) requires four boundary conditions: two of these follow from the symmetry of the problem,

$$\frac{\partial(H+h)}{\partial x}=\frac{\partial^3(H+h)}{\partial x^3}=0\quad\text{at}\quad x=0, \tag{67}$$

and the others are

$$h\to\bar{h},\quad \frac{\partial h}{\partial x}\to 0\quad\text{as}\quad |x|\to+\infty. \tag{68}$$

A. Numerical results

Equation (61) with its coefficients determined by (40), (41), (49), (54), and (66) was solved numerically with boundary conditions (67) and (68), using the method of lines,[52] for numerous initial conditions and in a wide range of the parameters involved. In all cases where the condensation criterion (1) was satisfied, a meniscus grew as $t\to\infty$.

A typical evolution is shown in Fig. 7, computed for the van der Waals fluid (42) and (43) with

$$T=0.1,\quad \varepsilon=0.02, \tag{69}$$

in which case the contact angle is $\tan\theta\approx 0.085\,9$. The corner was such that

$$\tan\frac{1}{2}(\pi-\phi)=0.1, \tag{70}$$

so that the vapor is weakly unstable. For simplicity, the bulk viscosity of vapor was assumed to be zero,

$$\mu_{b.v}=0, \tag{71}$$

whereas its nondimensional shear viscosity was chosen to match approximately the ratio of vapor and liquid viscosities of water at room temperature,

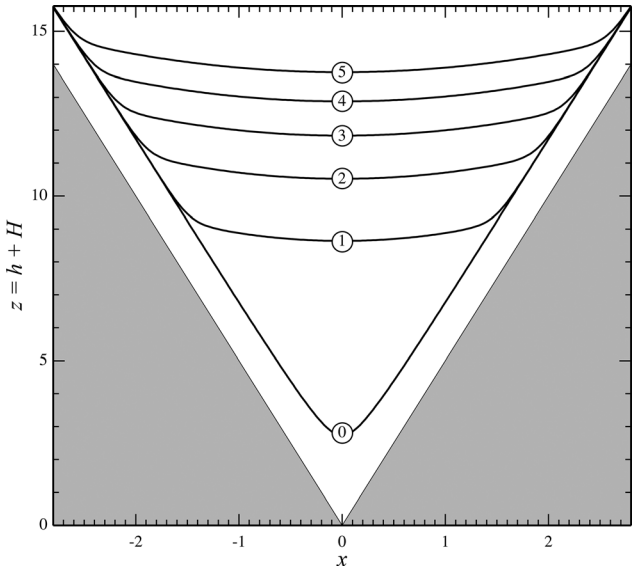

FIG. 7. An example of a meniscus growing in a sharp corner, for parameters (69)–(74). The curves show "snapshots" of the solution at $t = 300\,n$, where n is the curve number (thus, curve 0 is the initial condition).

$$\mu_{s.v} = 0.01. \tag{72}$$

The initial condition was

$$H + h = \sqrt{\left(\frac{x}{\varepsilon}\tan\frac{\pi-\phi}{2}\right)^2 + h_0 e^{-(x/\Delta_h)^2}} \quad \text{at} \quad t = 0, \tag{73}$$

with

$$h_0 = 1, \quad \Delta_h = 1 \tag{74}$$

[(73) looks similar to expression (59) for H, but they are not to be confused].

The following features of Fig. 7 should be observed:

(i) Initially, a quick adjustment occurs [reflected by the large difference between curves (0) and (1)].

(ii) At large times, the growth of the meniscus' thickness and the progress of its contact lines slow down.

Another feature is quantified in Fig. 8—which shows the thickness of the meniscus and the slope of the interface vs x for curve 5 of Fig. 7:

(iii) For large times, the "core" of the meniscus assumes a spherical-cup shape (under lubrication theory, this corresponds to a parabolic dependence of h on x).

Indeed, observe that, in the core, the interfacial slope changes *linearly* from 0 (horizontal interface) to

$$\frac{\partial(H+h)}{\partial x} = \frac{1}{\varepsilon}\left[\tan\frac{1}{2}(\pi-\phi) - \tan\theta\right] \tag{75}$$

(the angle between the interface and substrate equals θ). As seen in Fig. 8(b), $\partial(H+h)/\partial x$ assumes value (75) on the boundary separating

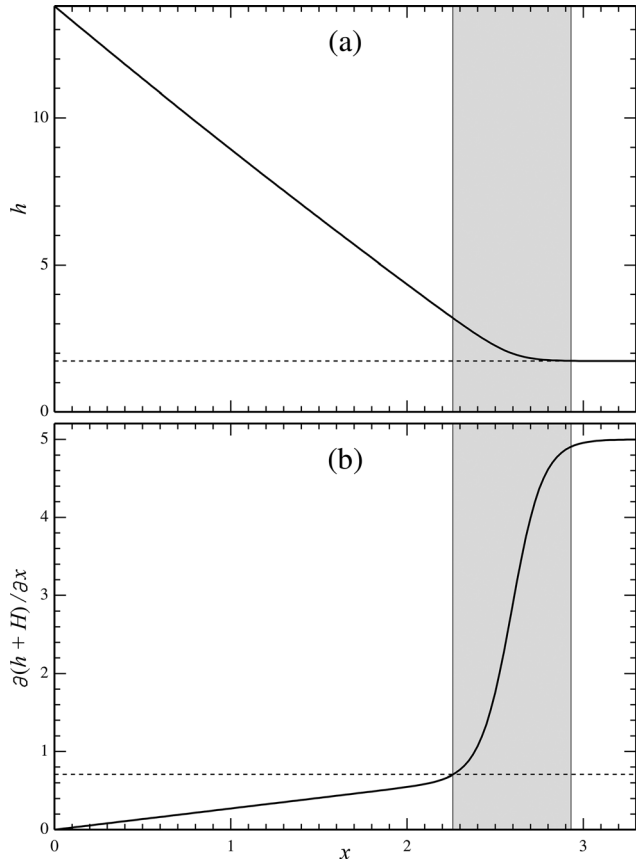

FIG. 8. The cross-section of the growing meniscus in a sharp corner, for parameters (69)–(74) and $t = 1500$ (corresponds to curve 5 in Fig. 7): (a) thickness of the meniscus, $h(x)$; (b) slope of the interface, $\partial(H+h)/\partial x$. The near-contact-line zone is shaded. The dotted line in panel (b) corresponds to the slope given by (75).

the core and the near-contact-line zone. In the latter, the thickness of the meniscus is close to that of the precursor film.

Figure 9 shows the typical evolution of a meniscus in a smoothed corner, computed for $H(x)$ given by (59) and (60) with

$$\tan\frac{\pi-\phi}{2} = 0.087\,1. \tag{76}$$

The fluid parameters are given by (69) and the initial condition by (73) with

$$h_0 = 3.5, \quad \Delta_h = 0.5. \tag{77}$$

Even though a steady solution exists in this case, the meniscus grows as $t \to \infty$. It would *not* grow and become static, only if the amplitude of the initial perturbation is sufficiently small—e.g., if $h_0 = 3.5$ in perturbation (77) is replaced with $h_0 \lesssim 2.9$. One should keep in mind, however, that, since h is nondimensionbalized by the interfacial thickness l, both these values of h_0 should be regarded microscopic.

Extensive numerical experiments with various initial conditions showed that, to make the meniscus grow, its initial volume has to be sufficiently high, but its shape is unimportant: if it is too "narrow" or

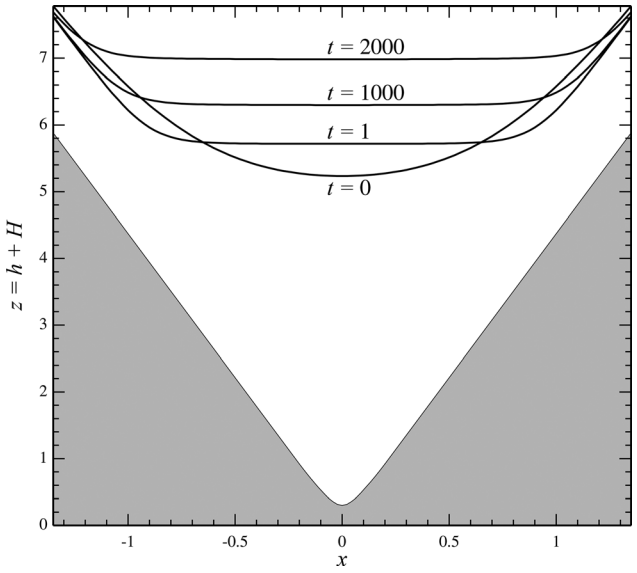

FIG. 9. An example of a growing meniscus in a smooth corner for parameters (59), (60), (69), (72), 73), (76), and (77). The times corresponding to the curves are shown in the figure (observe that they are not equally spaced).

too "wide," it spreads out or contracts, respectively. The end result of the adjustment is a meniscus with almost flat surface, with its further evolution depending on how wide it is. For growth, it should cover an area comparable to the smoothed part of the corner—otherwise it tends to the existing steady state and becomes static.

Most importantly, the adjusted meniscus does not have to be thick to initiate growth; its nondimensional thickness can be order-one. In dimensional terms, this means that the instability is triggered off by *microscopic* perturbations, i.e., those representing a liquid film whose thickness is comparable to the interfacial thickness.

As for the large-time evolution of menisci in a smoothed corner, it is qualitatively the same as that of their sharp-corner counterparts—i.e., both kinds of menisci demonstrate features (ii) and (iii).

B. The large-time behavior

Features (ii) and (iii) of the meniscus evolution listed in Subsection IV A allow one to deduce a simple asymptotic description of the large-time evolution.

Indeed, feature (iii) suggests that, as $t \to \infty$, the "outer" solution (in the meniscus core) is parabolic,

$$h - \bar{h} \sim h_0 - h_2 x^2 \quad \text{if} \quad x_{cl} - x \gg 1, \tag{78}$$

where $h_0(t)$ and $h_2(t)$ are undetermined functions, and $x_{cl}(t)$ is the approximate coordinate of the (right-hand) contact line—so that

$$h_0 - h_2 x_{cl}^2 = 0. \tag{79}$$

Since, at large times, the meniscus is thick and the contact line is far from the origin, one should assume $h_0 \gg 1$ and $x_{cl} \gg 1$, respectively.

According to feature (ii), the velocity of the contact line tends to zero with time—hence, the "inner" solution is close to that describing a *static* contact line. The latter is given by expression (52); setting in it $x_0 = x_{cl} + x_{00}$ (where x_{00} is an order-one constant), one obtains

$$h - \bar{h} \sim \frac{1}{C} \ln \left[1 + \exp \frac{C(x_{cl} + x_{00} - x)\tan\theta}{\varepsilon} \right] \quad \text{if} \quad x_{cl} - x \sim 1, \tag{80}$$

where the (order-one) constant x_{00} can only be found from higher-order approximations.

Matching the outer solution (78) to the inner solution (80) effectively amounts to matching their "slopes"; recalling then equality (79), one obtains

$$x_{cl} = \frac{2\varepsilon h_0}{\tan\theta}, \quad h_2 = \frac{\tan^2\theta}{4\varepsilon^2 h_0}. \tag{81}$$

It still remains to find $h_0(t)$—which can be done by either examining the higher order approximations of the inner and outer solutions—or, alternatively, through a simple shortcut involving the exact equation (61). To do the latter, integrate (61) with respect to x from 0 to ∞ and, recalling boundary conditions (67) and (68) and the fact that

$$\frac{dH}{dx} \to \frac{1}{\varepsilon} \tan \frac{\pi - \phi}{2} \quad \text{as} \quad x \to \infty, \tag{82}$$

obtain

$$\frac{dM}{dt} = \frac{1}{\varepsilon^2 A} \left[\frac{\sigma}{\varepsilon} \tan \frac{\pi - \phi}{2} - \int_0^\infty f(h - \bar{h}) dx \right], \tag{83}$$

where

$$M = \int_0^\infty (h - \bar{h}) dx \tag{84}$$

is the half-area of the meniscus cross section. Since the near-contact-line region is small, M can be estimated using the outer solution (78). Observe also that the function $f(h - \bar{h})$ [defined by (50)] is exponentially small in the outer region—hence, the integral on the right-hand side of equality (83) can be estimated using the inner solution (80). Carrying out both estimates and recalling equalities (81), one can reduce (83) and (84) to

$$\frac{dM}{dt} \to \frac{\sigma}{A\varepsilon^3} \left(\tan \frac{\pi - \phi}{2} - \tan\theta \right) \quad \text{as} \quad t \to \infty, \tag{85}$$

$$M \sim \frac{4\varepsilon h_0^2}{3\tan\theta} \quad \text{as} \quad t \to \infty. \tag{86}$$

Thus, the thickness h_0 of the meniscus grows as $t^{1/2}$, as does its width x_{cl} [due to (81)]—whereas the meniscus cross-sectional area grows linearly. It is also evident from equality (85) that the meniscus grows only subject to condition (1). It should be emphasized that asymptotic expressions (85) and (86) hold for both sharp and smoothed corners [if the latter satisfy condition (82)].

To test asymptotics (85), the exact equation (61) was solved numerically for large times. Typical results are illustrated in Fig. 10: one can see that the rate of growth of the cross-sectional area of the meniscus does converge to the predicted constant, albeit fairly slowly.

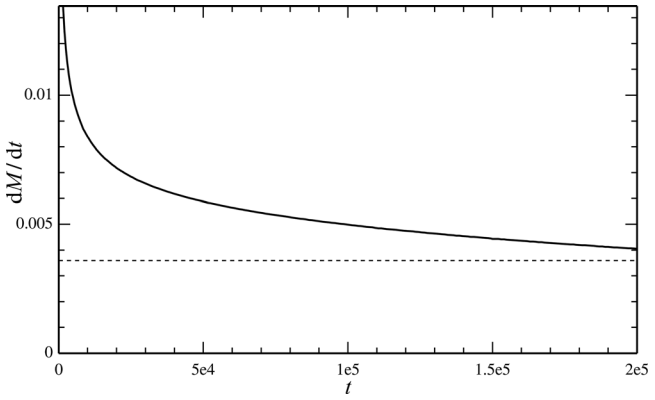

FIG. 10. The long-time evolution of a meniscus with parameters (69)–(74) (the same as in Fig. 7). M is the half-area of the cross-section [see expression (84)], t is the time. The horizontal dotted line represents the asymptotic value of dM/dt predicted by expression (85).

V. CHARACTERISTIC TIME OF THE KELVIN EFFECT

To estimate how quick the Kelvin effect is, one needs to rewrite Eq. (61) in terms of the dimensional variables and in a form minimizing the dependence on the fluid's thermodynamic properties (which may not be known in applications). The DIM parameters—the Korteweg constant K and the near-substrate density ρ_0—can be expressed through the surface tension and contact angle, respectively (for more details, see Ref. 47). The low-temperature assumption $T \ll 1$ will also be used as it is applicable to many common fluids (including water) at room temperature,[50] and it is also a precondition that $\rho_v \ll \rho_l$, which is required for Eq. (61) to hold.

Thus, reversing nondimensionalization (26)–(29), (B1)–(B4), and (B27) and retaining the same notation for the dimensional variables, one can write the three-dimensional analogue of Eq. (61) in the form

$$\frac{\partial h}{\partial t} + \sigma\nabla\cdot\left\{Q(h)\,\nabla\left[\nabla^2(H+h) - \frac{\tan^2\theta}{l}f\left(\frac{h-\bar{h}}{l}\right)\right]\right\} = \frac{\sigma}{0.14219\left(\mu_{b.v}+\frac{4}{3}\mu_{s.v}\right)}\left(\frac{\rho_v}{\rho_l}\right)^{5/2}\left(\frac{K\rho_l}{RT}\right)^{1/2} \times\left[\nabla^2(H+h) - \frac{\tan^2\theta}{l}f\left(\frac{h-\bar{h}}{l}\right)\right]. \tag{87}$$

The fluid parameters which appear in this equation and their typical values are listed in Table I. The function,

$$f(\xi) = (1-\mathrm{e}^{-\xi})\mathrm{e}^{-\xi},$$

is universal (does not involve any parameters), whereas the thickness of the precursor film $\bar{h}$ and interfacial thickness l depend on the fluid's chemical potential $G(\rho, T)$ and pressure $p(\rho, T)$,

$$l = K^{1/2}\left\{\left[\frac{\partial G(\rho,T)}{\partial\rho}\right]_{\rho=\rho_l}\right\}^{-1/2},$$

$$\bar{h} = K^{1/2}\int_{\frac{1}{2}(\rho_l+\rho_v)}^{\rho_0}\frac{2^{-1/2}\mathrm{d}\rho}{\sqrt{\rho[G(\rho,T)-G(\rho_v,T)]-p(\rho,T)+p(\rho_v,T)}}.$$

TABLE I. The fluid parameters involved in Eq. (87) and their typical values (at $T = 25^\circ$C and/or $p = 1$ atm, if appropriate). The values of the parameters not related to the DIM have been borrowed from Refs. 53–56, and the estimate of K, from Ref. 47.

Notation	Parameter	Value
ρ_l	Density (liquid)	$997.00\,\mathrm{kg\,m^{-3}}$ (water)
ρ_v	Density (vapor)	$0.023\,1\,\mathrm{kg\,m^{-3}}$ (water) $1.183\,9\,\mathrm{kg\,m^{-3}}$ (air)
R	Specific gas constant	$461.52\,\mathrm{m^2 s^{-2} K^{-1}}$ (water)
$\mu_{s.l}$	Shear viscosity (liquid)	$0.890\times10^{-3}\,\mathrm{Pa\,s}$ (water)
$\mu_{s.v}$	Shear viscosity (vapor)	$0.986\,7\times10^{-5}\,\mathrm{kg\,m^{-1}s^{-1}}$ (water) $1.837\,4\times10^{-5}\,\mathrm{kg\,m^{-1}s^{-1}}$ (air)
$\mu_{b.v}$	Bulk viscosity (vapor)	$2.738\,0\times10^{-5}\,\mathrm{kg\,m^{-1}s^{-1}}$ (water) $1.746\,6\times10^{-5}\,\mathrm{kg\,m^{-1}s^{-1}}$ (air)
σ	Surface tension	$72.06\,\mathrm{mN\,m^{-1}}$ (water/air)
K	The Korteweg constant	$2.45\times10^{-17}\,\mathrm{m^7 kg^{-1}s^{-2}}$ (water)

The coefficient $Q(h)$ can be expressed through the function $\bar{\rho}(z)$ describing a flat liquid/vapor interface in an unbounded space; $\bar{\rho}(z)$, in turn, is related to $G(\rho, T)$ through the following boundary-value problem:

$$K\frac{\mathrm{d}^2\bar{\rho}}{\mathrm{d}z^2} - G(\bar{\rho},T) + G(\rho_v,T) = 0,$$
$$\bar{\rho}(z)\to\rho_l \quad \text{as} \quad z\to-\infty,$$
$$\bar{\rho}(z)\to\rho_v \quad \text{as} \quad z\to+\infty,$$
$$\bar{\rho}(0) = \frac{1}{2}(\rho_l+\rho_v).$$

Once $\bar{\rho}(x)$ is computed, $Q(h)$ is given by

$$Q(h) = \frac{1}{\rho_l^2}\int_0^\infty\frac{\hat{\rho}^2(z-h)}{\mu_s(\bar{\rho}(z-h),T)}\mathrm{d}z,$$

where $\mu_s(\rho, T)$ is the fluid's shear viscosity, and

$$\hat{\rho}(z) = \int_z^\infty[\bar{\rho}(z')-\rho_v]\mathrm{d}z'.$$

To calculate $\bar{h}$, l, and $Q(h)$, one needs (typically, empiric) approximations of $G(\rho, T)$ and $p(\rho, T)$, which may not be available for the liquid used in a specific experiment (say, a certain type of silicone oil). Even for water—whose thermodynamic properties are well known—there is a problem ensuing from the dependence of l on the derivative $\partial G/\partial\rho$: even if $G(\rho, T)$ itself is approximated well, its derivative can be inaccurate (according to the experience of the author of the present paper).

Instead, one can treat l and $\bar{h}$ as adjustable parameters and fix their values by fitting the theoretical results to experimental data (which is how all other models of contact lines work without exception).

As for $Q(h)$, one can show that, to leading order, it reduces to

$$Q(h) = \frac{1}{\mu_{s.l}}\left(\frac{1}{3}h^3 + Q_0 l^3\right),$$

where Q_0 depends on $G(\rho, T)$ and $\mu_s(\rho, T)$. For the van der Waals fluid under an extra assumption that μ_s is proportional to ρ, the constant Q_0 happens to be small: $Q_0 \approx 0.098\,595$. Furthermore, since Eq. (87) was derived under the assumption that the ratio h/l is (logarithmically) large, the second term in the above expression is small. This claim has been verified by computations: in particular, the solutions in Figs. 7–9 have turned out to be indistinguishable from those computed for $Q_0 = 0$ or $Q_0 = 2 \times 0.098\,595$, with the rest of the parameters being the same. This suggests that one can simulate Eq. (87) with simply

$$Q(h) = \frac{1}{3\mu_{s.l}} h^3.$$

Note also that l, $\bar{h}$, and $Q(h)$ do not appear in the first term on the right-hand side of Eq. (87), which describes the Kelvin effect. This allows one to objectively estimate the characteristic time of the Kelvin effect, defined as

$$\tau = \frac{0.142\,19\left(\mu_{b.v} + \frac{4}{3}\mu_{s.v}\right)}{\sigma} \left(\frac{\rho_l}{\rho_v}\right)^{5/2} \left(\frac{RT}{K\rho_l}\right)^{1/2} L^2, \qquad (88)$$

where L is the horizontal scale of the liquid film.

To place this estimate in the context of one's everyday experience, τ will be estimated for the parameters of household mold: it is known to appear in corners and wall irregularities, and is generally a good example of Kelvin-effect-induced condensation. Thus, using the parameters of water for the liquid phase and those of air for the vapor, and letting $L = 0.1$ mm as the smallest visible mold size, one obtains $\tau \approx 11$ h. This estimate characterizes how quickly a wet spot would become visible if the air in one's dwelling is 100% humid.

One should keep in mind, however, that Eq. (87) and estimate (88) have been derived for a pure fluid—hence, using them for the water/air combination is somewhat inconsistent. To obtain a more reliable estimate, one needs an extension of the present results to multicomponent fluids, which is currently in progress. One should also take into account the absorption of the condensate by the wallpaper or plaster, as well as its consumption by bacteria (which turn the liquid into the actual mold).

Another potential application of the present results is liquid films in steam turbines, where the temperature can be as high as 400°C. The corresponding value of ρ_l/ρ_v is much smaller than that at room temperature, so that estimate (88) predicts that the condensation is quicker by several orders of magnitude.

VI. CONCLUDING REMARKS

This paper examined the evolution of saturated vapor between two intersecting walls, and its main physical result is condition (1). If the angle ϕ at which the walls intersects and the contact angle θ satisfy this condition, the vapor begins to condensate and a liquid meniscus starts to grow in the corner. If condition (1) does *not* hold, there is a steady (non-growing) solution describing a steady meniscus. Both these results have been obtained using Eq. (61) derived in Appendix B 1 under the assumptions that $\theta \ll 1$, $\phi \approx \pi$ (hydrophilic walls intersecting at an almost straight angle), and $\rho_v/\rho_l \ll 1$ (the vapor-to-liquid density ratio is small). For the regime $\rho_v/\rho_l \sim 1$, a separate asymptotic equation was derived, Eq. (B23) of Appendix B 2; its solutions have not been described in this paper as they are similar to those of Eq. (61).

The main mathematical results of the present paper are asymptotic equation (61) and its dimensional version (87). They were used to formally derive condition (1), but can also be employed for modeling thin drops with contact lines.

To understand in what way Eq. (87) differs from the existing liquid-film models incorporating evaporation (e.g., Refs. 3–8, 10, 14–19, and 57), note that there are two distinct mechanisms of evaporation of drops:

(a) through *diffusion* of vapor in the surrounding air, and
(b) through *advection* of vapor by the flow due to the variations of the chemical potential (caused by the curvature of the drop's surface).

All of the existing models are based on mechanism (a), whereas the present work, on mechanism (b). The latter is the only one acting in *pure* fluids, where diffusion does not occur.

In *multicomponent* fluids, however, both mechanisms should be accounted for—but, so far, only (a) has. This shortcoming can be remedied using the multicomponent DIM—or perhaps one of the models incorporating kinetic theory (see Ref. 58 and references therein).

ACKNOWLEDGMENTS

The author is grateful to Demetrios Papageorgiou for a helpful question and to Mikhail Benilov, for a helpful advice.

AUTHOR DECLARATIONS

Conflict of interest

The authors have no conflicts to disclose.

DATA AVAILABILITY

The data that support the findings of this study are available within the article.

APPENDIX A: ASYMPTOTIC DESCRIPTION OF STATIC MENISCI

For simplicity, the asymptotic analysis in both appendixes of this paper will be carried out for two-dimensional (2D) flow. The 3D versions of the equations derived can be easily deduced afterwards from the requirement of horizontal isotropy.

1. Preliminaries

In what follows, one needs, first, an expansion of the thickness $\bar{h}$ of the precursor film, and second, the large-distance asymptotics of the function $\bar{\rho}(z)$ describing a flat interface in an unbounded space.

(1) The Maxwell construction (20) and (21) and identity (5) imply

$$\rho[G(\rho, T) - G(\rho_v, T)] - p(\rho, T) + p(\rho_v, T) = \frac{C^2}{2}(\rho - \rho_l)^2 + \mathcal{O}\left[(\rho - \rho_l)^3\right] \quad \text{as} \quad \rho \to \rho_l, \qquad (A1)$$

where C is given by (41). Expansion (A1) implies that the integrand in expression (40) for $\bar{h}$ has a first-order pole at $\rho = \rho_l$; it is located

outside the integration interval, but not too far from its upper limit. Thus, (40) reduces to

$$\bar{h} = \bar{h}_0 + \bar{h}_1 + \mathcal{O}(\varepsilon), \tag{A2}$$

where

$$\bar{h}_0 = \frac{\ln \varepsilon^{-1}}{C}, \tag{A3}$$

$$\bar{h}_1 = \int_{\frac{1}{2}(\rho_l+\rho_v)}^{\rho_l} \left\{ \frac{2^{-1/2}}{\sqrt{\rho[G(\rho,T)-G(\rho_v,T)]-p(\rho,T)+p(\rho_v,T)}} - \frac{1}{C(\rho_l-\rho)} \right\} \mathrm{d}\rho + \frac{1}{C}\ln\frac{\rho_l-\rho_v}{2}. \tag{A4}$$

(2) It follows from the exact solution (38) that

$$\bar{\rho}(z) \sim \rho_l - \mathrm{e}^{C\left(z+\bar{h}_1\right)} \quad \text{as} \quad z \to -\infty,$$

where $\bar{h}_1$ is given by (A4). Then, using equalities (A2) and (A3), one can rewrite the above estimate in terms of the full thickness of the precursor film,

$$\bar{\rho}(z) \sim \rho_l - \varepsilon \mathrm{e}^{C(z+\bar{h})} \quad \text{as} \quad z \to -\infty. \tag{A5}$$

This expansion holds as long as its second term is smaller than the first one—i.e., for moderately (logarithmically) large distances, $-z \gtrsim \bar{h}$.

2. Derivation of Eq. (48)

The solution of Eq. (30) will be sought in the form

$$\rho(x,z) = \bar{\rho}(z-H-h) + \varepsilon^2\rho^{(2)} + \cdots, \tag{A6}$$

where $\bar{\rho}(z)$ describes a flat interface in an unbounded space and satisfies boundary-value problem (33)–(36). Physically, solution (A6) describes a slightly curved interface located at $z = H(x) + h(x)$ [i.e., at a height $h(x)$ above the substrate], and a small correction. In what follows, the two-term expansion (A6) plays an important role, for both static and evolving menisci.

Substituting (A6) into Eq. (30) and boundary condition (32) (boundary condition (31) will be discussed later), one obtains

$$\frac{\partial^2\rho^{(2)}}{\partial z^2} - \left(\frac{\partial G}{\partial \rho}\right)_{\rho=\bar{\rho}} \rho^{(2)} = \mathcal{R}, \tag{A7}$$

$$\rho^{(2)} \to 0 \quad \text{as} \quad z \to \infty, \tag{A8}$$

where

$$\mathcal{R} = -\frac{\partial^2\bar{\rho}}{\partial x^2}, \tag{A9}$$

and it is implied here (and in the rest of the paper, unless stated otherwise) that $\bar{\rho}$ depends on $z-H-h$, not just z.

(A7) is a linear nonhomogeneous second-order ordinary differential equation, and it can be readily verified that its homogeneous version is satisfied by $\rho^{(2)} = \partial\bar{\rho}/\partial z$. Thus, its general solution is easy to find: imposing boundary condition (A8), one obtains, after straightforward algebra,

$$\rho^{(2)} = \frac{\partial\bar{\rho}}{\partial z}\left[\int_z^{H+h}\left(\frac{\partial\bar{\rho}'}{\partial z}\right)^{-2} F(x,z')\,\mathrm{d}z' - h^{(2)}(x)\right], \tag{A10}$$

where $\bar{\rho}' = \bar{\rho}(z'-H-h)$,

$$F(x,z) = \int_z^{\infty} \frac{\partial\bar{\rho}'}{\partial z'}\mathcal{R}(x,z')\,\mathrm{d}z', \tag{A11}$$

and the undetermined function $h^{(2)}(x)$ is, mathematically, a constant of integration. Physically, $h^{(2)}$ corresponds to shifting the interface along the z axis by a distance of $\varepsilon^2 h^{(2)}$. In principle, it can be eliminated by replacing in expansion (A6) the leading-order solution $\bar{\rho}(z-H-h)$ with $\bar{\rho}(z-H-h-\varepsilon^2h^{(2)})$.

Expansion (A6) is valid if its second term $\varepsilon^2\rho^{(2)}$ is much smaller than the first term $\bar{\rho}$. This requirement clearly holds near the interface, where $z-H-h = \mathcal{O}(1)$—hence, $\rho^{(2)}$ does not involve any small or large parameters—hence, $\rho^{(2)} = \mathcal{O}(1)$. Furthermore, as shown below, the condition $\varepsilon^2\rho^{(2)} \ll \bar{\rho}$ holds near the substrate as well (even though $z-H-h$ can be large there, and so can $\rho^{(2)}$).

Thus, since expansion (A6) is uniformly applicable, there is no need to introduce a near-substrate boundary layer. Substituting expression (A10) into (A6) and then substituting the latter into boundary condition (31), one obtains

$$(\bar{\rho})_{z=H} + \varepsilon^2\left(\frac{\partial\bar{\rho}}{\partial z}\right)_{z=H}\left[\int_H^{H+h}\left(\frac{\partial\bar{\rho}}{\partial z}\right)^{-2} F(x,z)\,\mathrm{d}z - h^{(2)}\right] = \rho_l - \varepsilon. \tag{A12}$$

This is, essentially, the desired equation for $h(x)$. To reduce it to Eq. (48), one should assume that h is logarithmically large. Physically, such an assumption is not restrictive as liquid menisci are indeed thicker than the precursor film (describing *dry* substrate), and the thickness $\bar{h}$ of the latter *is* logarithmically large due to estimates (A2)–(A4). For large h, the main contribution to the integral in (A12) comes from the region adjacent to its lower limit, where $\partial\bar{\rho}/\partial z$ is small. Thus, one can use (A5) to obtain

$$\int_H^{H+h}\left(\frac{\partial\bar{\rho}}{\partial z}\right)^{-2} F(x,z)\,\mathrm{d}z = \frac{\varepsilon^{-2}}{2C^3}\mathrm{e}^{-2C(h-\bar{h})}F(x,H) + \mathcal{O}(\ln\varepsilon^{-1}). \tag{A13}$$

Given this estimate and (A5), the second term on the left-hand side of Eq. (A12) is $\mathcal{O}(\varepsilon)$—hence, it is much smaller than the first term. This justifies the use of expansion (A6) near the substrate. Substituting estimate (A13) into Eq. (A12) and using the large-distance asymptotics (A5) of $\bar{\rho}$ to simplify the rest of (A12), one can reduce it to leading order to

$$F(x,H) = 2C^2\left[1-\mathrm{e}^{-C(h-\bar{h})}\right]\mathrm{e}^{-C(h-\bar{h})}. \tag{A14}$$

Note that the undetermined function $h^{(2)}(x)$ does not appear in this (leading-order) equation; it can only be determined in the next order of the perturbation expansion. To close Eq. (A14), it remains to express F in terms of h. Backtracking through equalities (A11) and (A9) (thus, relating F to $\mathcal{R}$ to $\bar{\rho}$), one obtains

$$\int_H^\infty \frac{\partial\bar\rho}{\partial z}\left\{\frac{\mathrm{d}^2(H+h)}{\mathrm{d}z^2}\frac{\partial\bar\rho}{\partial z}-\left[\frac{\mathrm{d}(H+h)}{\mathrm{d}z}\right]^2\frac{\partial^2\bar\rho}{\partial z^2}\right\}\mathrm{d}z = 2C^2\left[1-\mathrm{e}^{-C(h-\bar h)}\right]\mathrm{e}^{-C(h-\bar h)}. \tag{A15}$$

Observe that, since h is large, it follows from the large-distance asymptotics (A5) that

$$\frac{\partial\bar\rho(z-H-h)}{\partial z}=\mathcal{O}(\varepsilon),\quad \frac{\partial^2\bar\rho(z-H-h)}{\partial z^2}=\mathcal{O}(\varepsilon)\quad \text{if}\quad z<H.$$

As a result, the lower limit of the integral in (A15) can be moved from H to $-\infty$ without introducing a leading-order error. After that, the second term on the left-hand side of Eq. (A15) vanishes, and (A15) turns into Eq. (48) as required.

APPENDIX B: ASYMPTOTIC EQUATIONS FOR EVOLVING MENISCI

As mentioned in the main body of the paper, there are two asymptotic regimes in this problem, depending on the parameter ρ_v/ρ_l. The common part of their analyses will be presented first, with the regime-specific parts to follow.

To nondimensionalize the governing equations, assume that the shear and bulk viscosities are of the same order, $\mu_s\sim\mu_b$, and introduce a scale μ representing them both. As shown by Ref. 46 for a flat substrate, the scale for the horizontal velocity u is determined by the balance of the viscous and Korteweg stresses, so that

$$U=\frac{\varepsilon^3 Pl}{\mu}, \tag{B1}$$

where ϱ, P, and l have been defined in the beginning of Sec. III. The scale for the vertical velocity w is regime-specific and will be chosen later—as is, and will be, the timescale.

In addition to the nondimensional variables defined by (26)–(29), introduce

$$u_{nd}=\frac{u}{U}, \tag{B2}$$

$$c_{nd}=\frac{c}{R},\quad B_{nd}=\frac{B}{P},\quad s_{nd}=\frac{s}{R}, \tag{B3}$$

$$(\mu_s)_{nd}=\frac{\mu_s}{\mu},\quad (\mu_b)_{nd}=\frac{\mu_b}{\mu},\quad \kappa_{nd}=\frac{\kappa}{\varkappa}, \tag{B4}$$

where $\varkappa$ is a characteristic scale of the thermal conductivity, and the specific gas constant R is that of the specific heat capacity c.

1. Regime 1: $\rho_v\sim\rho_l$

Let the nondimensional time and vertical velocity be

$$t_{nd}=\frac{t}{l/(\varepsilon^{-1}U)},\quad w_{nd}=\frac{w}{\varepsilon^{-1}U}. \tag{B5}$$

Substituting (26)–(29) and (B2)–(B5) into the 2D version of boundary-value problem (9)–(19), and omitting the subscript $_{nd}$, one obtains

$$\frac{\partial\rho}{\partial t}+\varepsilon^2\frac{\partial(\rho u)}{\partial x}+\frac{\partial(\rho w)}{\partial z}=0, \tag{B6}$$

$$\begin{aligned}\alpha\varepsilon^4\left(\frac{\partial u}{\partial t}+\varepsilon^2 u\frac{\partial u}{\partial x}+w\frac{\partial u}{\partial z}\right)+s\frac{\partial T}{\partial x}+\frac{\partial}{\partial x}\left(G-\varepsilon^2\frac{\partial^2\rho}{\partial x^2}-\frac{\partial^2\rho}{\partial z^2}\right)\\ =\frac{\varepsilon^2}{\rho}\left\{\frac{\partial}{\partial x}\left[2\varepsilon^2\mu_s\frac{\partial u}{\partial x}+\left(\mu_b-\frac{2\mu_s}{3}\right)\left(\varepsilon^2\frac{\partial u}{\partial x}+\frac{\partial w}{\partial z}\right)\right]\right.\\ \left.+\frac{\partial}{\partial z}\left[\mu_s\left(\frac{\partial u}{\partial z}+\frac{\partial w}{\partial x}\right)\right]\right\},\end{aligned} \tag{B7}$$

$$\begin{aligned}\alpha\varepsilon^4\left(\frac{\partial w}{\partial t}+\varepsilon^2 u\frac{\partial w}{\partial x}+w\frac{\partial w}{\partial z}\right)+s\frac{\partial T}{\partial z}+\frac{\partial}{\partial z}\left(G-\varepsilon^2\frac{\partial^2\rho}{\partial x^2}-\frac{\partial^2\rho}{\partial z^2}\right)\\ =\frac{\varepsilon^4}{\rho}\frac{\partial}{\partial x}\left[\mu_s\left(\frac{\partial u}{\partial z}+\frac{\partial w}{\partial x}\right)\right]\\ +\frac{\varepsilon^2}{\rho}\frac{\partial}{\partial z}\left[2\mu_s\frac{\partial w}{\partial z}+\left(\mu_b-\frac{2\mu_s}{3}\right)\left(\varepsilon^2\frac{\partial u}{\partial x}+\frac{\partial w}{\partial z}\right)\right],\end{aligned} \tag{B8}$$

$$\begin{aligned}\alpha\gamma\rho c\left(\frac{\partial T}{\partial t}+\varepsilon^2 u\frac{\partial T}{\partial x}+w\frac{\partial T}{\partial z}\right)+\beta B\left(\varepsilon^2\frac{\partial u}{\partial x}+\frac{\partial w}{\partial z}\right)\\ =\beta\varepsilon^2\left\{\mu_s\left[2\varepsilon^4\left(\frac{\partial u}{\partial x}\right)^2+\varepsilon^2\left(\frac{\partial u}{\partial z}+\frac{\partial w}{\partial x}\right)^2+2\left(\frac{\partial w}{\partial z}\right)^2\right]\right.\\ \left.+\left(\mu_b-\frac{2\mu_s}{3}\right)\left(\varepsilon^2\frac{\partial u}{\partial x}+\frac{\partial w}{\partial z}\right)^2\right\}\\ +\frac{\partial}{\partial x}\left(\kappa\frac{\partial T}{\partial x}\right)+\frac{1}{\varepsilon^2}\frac{\partial}{\partial z}\left(\kappa\frac{\partial T}{\partial z}\right),\end{aligned} \tag{B9}$$

$$u=0,\quad w=0\quad \text{at}\quad z=H, \tag{B10}$$

$$\frac{\partial u}{\partial z}\to 0,\quad \frac{\partial w}{\partial z}\to 0\quad \text{as}\quad z\to\infty, \tag{B11}$$

$$\rho=\rho_l-\varepsilon,\quad T=T_0\quad \text{at}\quad z=H, \tag{B12}$$

$$\rho\to\rho_v,\quad \frac{\partial T}{\partial z}\to 0\quad \text{as}\quad z\to\infty, \tag{B13}$$

where

$$\alpha=\frac{K\varrho^3}{\mu^2},\quad \beta=\frac{P\varrho^2K}{\mu\varkappa(T_0)_d},$$
$$\gamma=\frac{R\mu}{\varkappa},\quad T_0=\frac{\varrho R(T_0)_d}{P},$$

and $(T_0)_d$ is the dimensional temperature of the substrate.

The positions where α appears in Eqs. (B7) and (B8) suggest that it represents the Reynolds number, β is the "isothermality parameter" introduced by Ref. 50, and γ is the Prandtl number. For generality, these parameters are assumed to be order one (as shown by Ref. 50, they are typically either that or small).

Observe that Eq. (B9) involves a term proportional to $1/\varepsilon^2$, which cancels only if

$$T=T_0+\varepsilon^2\tilde T, \tag{B14}$$

i.e., the temperature variations are small. This does not mean, however, that their effect on the film dynamics is negligible. To make it such, one should also assume the isothermality parameter β to be also small.[46]

Substituting (B14) into Eq. (B8) and simplifying the notation by changing $T_0\to T$, one obtains

$$\frac{\partial}{\partial z}\left(\frac{\partial^2\rho}{\partial z^2}-G\right)=\varepsilon^2\left[\frac{\partial}{\partial z}\left(-\frac{\partial^2\rho}{\partial x^2}+\frac{\partial G}{\partial T}\tilde{T}\right)+s(T,\rho)\frac{\partial\tilde{T}}{\partial z}-\frac{1}{\rho}\frac{\partial}{\partial z}\left(\lambda\frac{\partial w}{\partial z}\right)\right]+\mathcal{O}(\varepsilon^4), \tag{B15}$$

where the effective viscosity $\lambda(\rho,T)$ is given by

$$\lambda(\rho,T)=\mu_b(\rho,T)+\frac{4}{3}\mu_s(\rho,T). \tag{B16}$$

For evolving menisci, the film thickness h depends on x and t (not just on x as in the static case). Keeping this in mind while substituting (A6) into (B15), one obtains

$$\frac{\partial^2\rho^{(2)}}{\partial z^2}-\left(\frac{\partial G}{\partial\rho}\right)_{\rho=\bar{\rho}}=\varepsilon^2\mathcal{R}_1, \tag{B17}$$

where

$$\mathcal{R}_1=-\frac{\partial^2\bar{\rho}}{\partial x^2}+\frac{\partial G(\bar{\rho},T)}{\partial T}\tilde{T}-\frac{\partial G(\rho_v,T)}{\partial T}(\tilde{T})_{z\to\infty}-\int_z^\infty\left\{s(\bar{\rho}',T)\frac{\partial\tilde{T}'}{\partial z'}-\frac{1}{\bar{\rho}'}\frac{\partial}{\partial z'}\left[\lambda(\bar{\rho}',T)\frac{\partial w'}{\partial z'}\right]\right\}\mathrm{d}z', \tag{B18}$$

and $\tilde{T}'=\tilde{T}(x,z',t)$, $w'=w(x,z',t)$, etc. Evidently, the left-hand side of Eq. (B17) coincides with that of its static counterpart (A7), and the boundary conditions for the two equations also coincide. Thus, the asymptotic equation for evolving menisci can be obtained by simply replacing $\mathcal{R}$ with $\mathcal{R}_1$ in the static equations (A11) and (A14), which yield

$$\int_H^\infty\frac{\partial\bar{\rho}}{\partial z}\mathcal{R}_1(x,z)\,\mathrm{d}z=2C^2\left[1-\mathrm{e}^{-C(h-\bar{h})}\right]\mathrm{e}^{-C(h-\bar{h})}. \tag{B19}$$

Next, substitute expression (B18) for $\mathcal{R}_1$ into the above equality, and then eliminate the integration with respect to z' by integrating by parts the term involving curly brackets. Recall also that h is large (as assumed in Appendix A), which implies

$$[\bar{\rho}(z-H-h)]_{z=H}=\rho_l+\mathcal{O}(\varepsilon). \tag{B20}$$

Thus, to leading order, one can rearrange (B19) into

$$-\int_H^\infty\frac{\partial\bar{\rho}}{\partial z}\frac{\partial^2\bar{\rho}}{\partial x^2}\mathrm{d}z+\int_H^\infty\left[\frac{\partial\bar{\rho}}{\partial z}\frac{\partial G(\bar{\rho},T)}{\partial T}\tilde{T}-\bar{\rho}s(\bar{\rho},T)\frac{\partial\tilde{T}}{\partial z}\right]\mathrm{d}z+\rho_l\int_H^\infty s(\bar{\rho},T)\frac{\partial\tilde{T}}{\partial z}\mathrm{d}z-(\rho_v-\rho_l)\frac{\partial G(\rho_v,T)}{\partial T}(\tilde{T})_{z\to\infty}-\rho_l\int_H^\infty\frac{\lambda(\bar{\rho},T)}{\bar{\rho}^2}\frac{\partial\bar{\rho}}{\partial z}\frac{\partial w}{\partial z}\mathrm{d}z=2C^2\left[1-\mathrm{e}^{-C(h-\bar{h})}\right]\mathrm{e}^{-C(h-\bar{h})}. \tag{B21}$$

To obtain a closed equation for h, the unknowns $\tilde{T}$ and w should be expressed in terms of $\bar{\rho}(z-H-h)$—which is not difficult, as it needs to be done to leading order only. Retaining, thus, the leading-order terms in Eqs. (B6), (B9), and (B10)–(B13), and changing $T_0\to T$, one obtains

$$\frac{\partial\bar{\rho}}{\partial t}+\frac{\partial(\bar{\rho}w)}{\partial z}=0,\qquad -\beta B(\bar{\rho},T)\frac{\partial w}{\partial z}+\frac{\partial}{\partial z}\left[\kappa(\bar{\rho},T)\frac{\partial\tilde{T}}{\partial z}\right]=0,$$
$$w=0,\quad \tilde{T}=0\quad\text{at}\quad z=H,\qquad \frac{\partial w}{\partial z}\to0,\quad\frac{\partial\tilde{T}}{\partial z}\to0\quad\text{as}\quad z\to\infty.$$

Keeping in mind estimate (B20) and recalling definition (8) of $B(\rho,T)$, one can deduce that, to leading order,

$$w=\frac{\partial h}{\partial t}\frac{\bar{\rho}-\rho_l}{\bar{\rho}},\qquad \tilde{T}=-\beta T\rho_l\frac{\partial h}{\partial t}\int_H^z\frac{s(\bar{\rho}',T)-s(\rho_v,T)}{\kappa(\bar{\rho}',T)}\mathrm{d}z'. \tag{B22}$$

Substituting these expressions into Eq. (B21), one obtains, after straightforward algebra,

$$(A+\beta D)\frac{\partial h}{\partial t}=\sigma\frac{\partial^2(H+h)}{\partial x^2}-2C^2\left[1-\mathrm{e}^{-C(h-\bar{h})}\right]\mathrm{e}^{-C(h-\bar{h})}, \tag{B23}$$

where

$$\sigma=\int_H^\infty\left(\frac{\partial\bar{\rho}}{\partial z}\right)^2\mathrm{d}z,\quad A=\rho_l^2\int_H^\infty\frac{\lambda(\bar{\rho},T)}{\bar{\rho}^4}\left(\frac{\partial\bar{\rho}}{\partial z}\right)^2\mathrm{d}z, \tag{B24}$$

$$D=T\rho_l^2\int_H^\infty\left[s(\bar{\rho},T)-s(\rho_v,T)-\frac{\rho_l-\rho_v}{\rho_l}\left(\rho\frac{\partial s}{\partial\rho}\right)_{\rho=\rho_v}\right]\times\frac{s(\bar{\rho},T)-s(\rho_v,T)}{\kappa(\bar{\rho},T)}\mathrm{d}z. \tag{B25}$$

(B23) is the desired asymptotic equation describing menisci with order-one vapor-to-liquid density ratio, but its coefficients can be simplified further, similar to how it was done in Appendix A. Moving the lower limit of integration in (B24) from H to $-\infty$, one can reduce σ to its standard form, (49), and A, to

$$A=\rho_l^2\int_{-\infty}^\infty\frac{\lambda(\bar{\rho},T)}{\bar{\rho}^4}\left(\frac{\partial\bar{\rho}}{\partial z}\right)^2\mathrm{d}z. \tag{B26}$$

The integrand in (B25), in turn, tends to a constant as $z\to-\infty$, so the lower limit cannot be moved to $-\infty$. One can still simplify (B25) by integrating it by parts and *then* moving the limit to $-\infty$. Eventually, (B25) becomes

$$D=D_1h-D_2,$$

where

$$D_1=T\rho_l^2\left[s(\rho_l,T)-s(\rho_v,T)-\left(1-\frac{\rho_v}{\rho_l}\right)\left(\rho\frac{\partial s}{\partial\rho}\right)_{\rho=\rho_v}\right]\times\frac{s(\rho_l,T)-s(\rho_v,T)}{\kappa(\rho_l,T)},$$

$$D_2=T\rho_l^2\int_{-\infty}^\infty z\frac{\partial}{\partial z}\left\{\left[s(\bar{\rho},T)-s(\rho_v,T)-\frac{\rho_l-\rho_v}{\rho_l}\left(\rho\frac{\partial s}{\partial\rho}\right)_{\rho=\rho_v}\right]\times\frac{s(\bar{\rho},T)-s(\rho_v,T)}{\kappa(\bar{\rho},T)}\right\}\mathrm{d}z.$$

2. Regime 2: $\rho_v \ll \rho_l$

Let ρ_v be small. Then, according to (B22), the vertical velocity w in the vapor phase is large. This makes sense physically: a large density difference between vapor and liquid implies a faster evaporative flow. Mathematically though, the growth of w makes the scaling inconsistent, suggesting that a boundary layer exists between the asymptotic regions describing liquid and vapor.

Thus, three asymptotic regions are expected to arise in the problem: the liquid region where $\rho \sim \rho_l$, the boundary layer where $\rho \sim \rho_v$, and the vapor region where $\rho \approx \rho_v$. The last one is trivial and has no impact on the global dynamics—hence, will not be discussed.

a. The liquid region

The nondimensional time and vertical velocity in this region are defined by

$$t_{nd} = \frac{t}{l/(\varepsilon U)}, \quad w_{nd} = \frac{w}{\varepsilon U}, \tag{B27}$$

where U is given by (B1). Substituting (26)–(29), (B2)–(B4), and (B27) into the 2D version of the governing set (9)–(13), one obtains (the subscript $_{nd}$ omitted),

$$\frac{\partial \rho}{\partial t} + \frac{\partial(\rho u)}{\partial x} + \frac{\partial(\rho w)}{\partial z} = 0, \tag{B28}$$

$$\begin{aligned}
&\alpha\varepsilon^6\left(\frac{\partial u}{\partial t} + u\frac{\partial u}{\partial x} + w\frac{\partial u}{\partial z}\right) + s\frac{\partial T}{\partial x} + \frac{\partial}{\partial x}\left(G - \varepsilon^2\frac{\partial^2\rho}{\partial x^2} - \frac{\partial^2\rho}{\partial z^2}\right)\\
&= \frac{\varepsilon^4}{\rho}\frac{\partial}{\partial x}\left[2\mu_s\frac{\partial u}{\partial x} + \left(\mu_b - \frac{2\mu_s}{3}\right)\left(\frac{\partial u}{\partial x} + \frac{\partial w}{\partial z}\right)\right]\\
&\quad + \frac{\varepsilon^2}{\rho}\frac{\partial}{\partial z}\left[\mu_s\left(\frac{\partial u}{\partial z} + \varepsilon^2\frac{\partial w}{\partial x}\right)\right],
\end{aligned} \tag{B29}$$

$$\begin{aligned}
&\alpha\varepsilon^8\left(\frac{\partial w}{\partial t} + u\frac{\partial w}{\partial x} + w\frac{\partial w}{\partial z}\right) + s\frac{\partial T}{\partial z} + \frac{\partial}{\partial z}\left(G - \varepsilon^2\frac{\partial^2\rho}{\partial x^2} - \frac{\partial^2\rho}{\partial z^2}\right)\\
&= \frac{\varepsilon^4}{\rho}\left\{\frac{\partial}{\partial x}\left[\mu_s\left(\frac{\partial u}{\partial z} + \varepsilon^2\frac{\partial w}{\partial x}\right)\right]\right.\\
&\quad \left. + \frac{\partial}{\partial z}\left[2\mu_s\frac{\partial w}{\partial z} + \left(\mu_b - \frac{2\mu_s}{3}\right)\left(\frac{\partial u}{\partial x} + \frac{\partial w}{\partial z}\right)\right]\right\},
\end{aligned} \tag{B30}$$

$$\begin{aligned}
&\alpha\gamma\rho c\left(\frac{\partial T}{\partial t} + u\frac{\partial T}{\partial x} + w\frac{\partial T}{\partial z}\right) + \beta B\left(\frac{\partial u}{\partial x} + \frac{\partial w}{\partial z}\right)\\
&= \beta\varepsilon^2\left\{\mu_s\left[2\varepsilon^2\left(\frac{\partial u}{\partial x}\right)^2 + \left(\frac{\partial u}{\partial z} + \varepsilon^2\frac{\partial w}{\partial x}\right)^2 + 2\varepsilon^2\left(\frac{\partial w}{\partial z}\right)^2\right]\right.\\
&\quad \left. + \varepsilon^2\left(\mu_b - \frac{2\mu_s}{3}\right)\left(\frac{\partial u}{\partial x} + \frac{\partial w}{\partial z}\right)^2\right\}\\
&\quad + \frac{1}{\varepsilon^2}\frac{\partial}{\partial x}\left(\kappa\frac{\partial T}{\partial x}\right) + \frac{1}{\varepsilon^4}\frac{\partial}{\partial z}\left(\kappa\frac{\partial T}{\partial z}\right).
\end{aligned} \tag{B31}$$

The boundary conditions for this set coincide with their regime-1 counterparts (B10)–(B13). The temperature equation (B31) suggests that

$$T = T_0 + \mathcal{O}(\varepsilon^4), \tag{B32}$$

with the implication that the temperature variations are too small to affect the leading-order dynamics [compare (B32) to its regime-1 counterpart (B14)]. Thus, the temperature equation can be simply omitted, and in the rest of the governing set, one can let $T = \text{const}$. Given the quasi-isothermality condition (B32), it follows from equation (B30) that

$$G(\rho, T) - G(\rho_v, T) - \varepsilon^2\frac{\partial^2\rho}{\partial x^2} - \frac{\partial^2\rho}{\partial z^2} = \varepsilon^2 G_0 + \mathcal{O}(\varepsilon^4), \tag{B33}$$

where $G_0(x, t)$ is an undetermined function. To relate it to $h(x, t)$, one should use the two-term expansion (A6), after which (B33) yields

$$\frac{\partial^2\rho^{(2)}}{\partial z^2} - \left(\frac{\partial G}{\partial \rho}\right)_{\rho=\bar{\rho}} = -\frac{\partial^2\bar{\rho}}{\partial x^2} - G_0. \tag{B34}$$

Following the same reasoning as that in regime 1, but keeping in mind that, this time, $\rho_v \ll 1$, one can deduce from the boundary condition for ρ at the substrate that

$$G_0 = -\frac{1}{\rho_l}\left\{\sigma\frac{\partial^2(H+h)}{\partial x^2} - 2C^2\left[1 - \mathrm{e}^{-C(h-\bar{h})}\right]\mathrm{e}^{-C(h-\bar{h})}\right\}. \tag{B35}$$

Next, substitute (B32) and (B33) into Eq. (B29) for u. Keeping in mind that u should satisfy the no-slip condition at the substrate and the no-viscous-stress condition at infinity, one obtains

$$u = -\frac{\partial G_0}{\partial x}\int_H^z \frac{\hat{\rho}'}{\mu_s(\bar{\rho}', T)}\mathrm{d}z' + \mathcal{O}(\varepsilon^2), \tag{B36}$$

where $\hat{\rho}$ is related to $\bar{\rho}$ by equality (64). Finally, substitute (B36) into Eq. (B28) and solve the latter for w, subject to the no-through-flow requirement at the substrate,

$$w = \frac{\partial h}{\partial t}\left(1 - \frac{\rho_l}{\bar{\rho}}\right) + \frac{1}{\bar{\rho}}\frac{\partial}{\partial x}\left[\frac{\partial G_0}{\partial x}\int_H^z \frac{(\hat{\rho}' - \hat{\rho})\hat{\rho}'}{\mu_s(\bar{\rho}', T)}\mathrm{d}z'\right] + \mathcal{O}(\varepsilon^2). \tag{B37}$$

If the $\bar{\rho}$ is small, this expression is evidently large—suggesting, as expected, the existence of a boundary layer.

b. The boundary layer

To obtain the solution in the boundary layer, the liquid-region equations (B28)–(B31) need to be rescaled. The parameters of the new variables have to be first guessed and then verified through matching to the liquid region.

The boundary layer will be described by the following inner variables:

$$z_i = \frac{z - Z(x, t)}{\rho_v^{1/2}}, \quad \rho_i = \frac{\rho}{\rho_v},$$

where $Z(x, t)$ is the height of the boundary layer. The horizontal coordinate x and time t do not need to be rescaled (their scales in the boundary layer are forced by the liquid's dynamics). Given that, in the end, the two regions will be matched, the boundary-layer

scaling for w can be deduced from the small-$\bar{\rho}$ asymptotics of the liquid-region solution (B37), which suggests

$$w_i = \rho_v w.$$

As for the horizontal velocity u, the liquid-region solution (B36) implies that u remains order-one when $\bar{\rho} \to 0$—hence, in the boundary layer, u does not need to be rescaled.

One can also take advantage of two physical assumptions. Since the fluid density in the boundary layer is small, one can safely assume that the chemical potential there is that of ideal gas,

$$G(\rho, T) = T \ln \rho \quad \text{if} \quad \rho \sim \rho_v.$$

In addition, both kinetic theory (e.g., Ref. 59) and measurements (e.g., Ref. 53) suggest that the vapor viscosity and thermal conductivity are independent of the density—thus, to leading order, one can assume

$$\mu_s(\rho, T) = \mu_{s.v}(T), \quad \mu_b(\rho, T) = \mu_{b.v}(T),$$
$$\kappa(\rho, T) = \kappa_v(T) \quad \text{if} \quad \rho \sim \rho_v.$$

Note that the viscosity and thermal conductivity of vapor are typically much smaller than those of liquid—hence, $\mu_{s.v}$, $\mu_{b.v}$, and κ_v are small parameters (in addition to ε and ρ_v).

The following asymptotic limit is assumed:

$$\varepsilon^2 \rho_v^{-5/2} \mu_v = \mathcal{O}(1) \quad \text{as} \quad \varepsilon, \rho_v, \mu_v, \kappa_v \to 0, \tag{B38}$$

where μ_v is, say, $(\mu_{s.v} + \mu_{b.v})/2$. As seen later, (B38) is a characteristic limit of regime 2 and, thus, covers adjacent situations, $\varepsilon^2 \rho_v^{-5/2} \mu_v \gg 1$ and $\varepsilon^2 \rho_v^{-5/2} \mu_v \ll 1$, as well. Note also that, as suggested by measurements,[53]

$$\kappa_v \sim \mu_v \gg \rho_v.$$

Summarizing the above estimates, assumptions, and scaling, one can deduce from the temperature equation (B32) the following quasi-isothermality condition:

$$T = T_0 + \mathcal{O}\left(\varepsilon^4 \frac{\rho_v^3}{\mu_v^2 \kappa_v}\right),$$

which is even stronger than its liquid-region counterpart (B32).

Rewriting Eqs. (B28) and (B30) in terms of the new variables, omitting Eq. (B29) for u (which will not be needed), and replacing the temperature equation with $T = \text{const}$, one obtains

$$\frac{\partial(\rho_i w_i)}{\partial z_i} = \mathcal{O}(\rho_v^{3/2}), \tag{B39}$$

$$\frac{\partial}{\partial z_i}\left[T \ln \rho_i - \varepsilon^2 \left(\frac{\partial Z}{\partial x}\right)^2 \frac{\partial^2 \rho_i}{\partial z_i^2} - \frac{\partial^2 \rho_i}{\partial z_i^2}\right] = \varepsilon^2 \left[\frac{\varepsilon^2 \rho_v^{-5/2}\left(\mu_{b.v} + \frac{4}{3}\mu_{s.v}\right)}{\rho_i} \frac{\partial^2 w_i}{\partial z_i^2} + \mathcal{O}(\rho_v^{3/2})\right]. \tag{B40}$$

Observe that w_i appears in Eq. (B40) only as a perturbation, which is why Eq. (B39) includes the leading-order term only.

Equation (B39) yields $\rho_i w_i = \text{const}$, where the constant can be determined by matching w_i to the small-$\bar{\rho}$ limit of the liquid-region solution (B37). Keeping in mind that $\hat{\rho}(z)$ is also small [because $\bar{\rho}(z)$ is small—see (64)], one obtains

$$w = -\frac{\rho_l}{\bar{\rho}}\left\{\frac{\partial h}{\partial t} - \rho_l \frac{\partial}{\partial x}\left[\frac{\partial G_0}{\partial x} Q(h)\right]\right\}. \tag{B41}$$

ρ_i should be sought in the form of a two-term expansion,

$$\rho_i = \bar{\rho}_i(z_i) + \varepsilon^2 \rho_i^{(2)} + \cdots, \tag{B42}$$

where $\bar{\rho}_i(z_i)$ satisfies the following boundary-value problem:

$$\frac{\mathrm{d}^2 \rho_i}{\mathrm{d} z_i^2} - T \ln \bar{\rho}_i = 0, \tag{B43}$$

$$\bar{\rho} \to \infty \quad \text{as} \quad z' \to -\infty, \tag{B44}$$

$$\bar{\rho} \to 1 \quad \text{as} \quad z' \to +\infty. \tag{B45}$$

Physically, $\bar{\rho}_i$ describes the small-density part of a flat interface in an unbounded space—hence, it is the small-ρ_v limit of the function $\bar{\rho}$ defined previously.

Substitution of (B42) into Eq. (B40) yields

$$\frac{\partial^2 \rho_i^{(2)}}{\partial z_i^2} - \frac{T}{\bar{\rho}_i} \rho_i^{(2)} = -\left(\frac{\partial Z}{\partial x}\right)^2 \frac{\partial^2 \bar{\rho}_i}{\partial z_i^2} + \int_{z_i}^{\infty} \frac{\varepsilon^2 \rho_v^{-5/2}\left(\mu_{b.v} + \frac{4}{3}\mu_{s.v}\right)}{\rho_i} \frac{\partial^2 w_i}{\partial z_i^2} \mathrm{d} z_i. \tag{B46}$$

The solution of this equation, $\rho_i^{(2)}$, should be matched to its liquid-region counterpart $\rho^{(2)}$ (the first terms in the two expansions match automatically as they both describe a flat interface in an unbounded space). Instead of $\rho_i^{(2)}$ and $\rho^{(2)}$, however, it is much simpler to match the right-hand sides of the equations determining them: (B46) for $\rho_i^{(2)}$ and (B34) for $\rho^{(2)}$ [the left-hand sides of these equations match automatically under the assumption that $G(\rho, T) \sim T \ln \rho$ as $\rho \to 0$]. Keeping in mind that that w_i is given by expression (B41), one obtains

$$\left(\frac{\partial Z}{\partial x}\right)^2 = \left[\frac{\partial (H + h)}{\partial x}\right]^2,$$
$$-G_0 = \varepsilon^2 \rho_v^{-5/2}\left(\mu_{b.v} + \frac{4\mu_{s.v}}{3}\right)\left\{\frac{\partial h}{\partial t} - \rho_l \frac{\partial}{\partial x}\left[\frac{\partial G_0}{\partial x} Q(h)\right]\right\} \times \int_{-\infty}^{\infty} \frac{1}{\bar{\rho}_i} \frac{\partial^2}{\partial z_i^2}\left(-\frac{1}{\bar{\rho}_i}\right) \mathrm{d} z_i. \tag{B47}$$

The former equality implies $Z = H + h + \text{const}$, which means that the boundary layer is pinned to a certain point of the interfacial profile. This point is determined by const, which can be found only from the next order of the perturbation expansion (and does not affect the leading-order solution). Finally, using (B35) to eliminate G_0 from Eq. (B47), one obtains the desired equation for $h(x, t)$—which can be written in form (61) with

$$A = \rho_l^2 \rho_v^{-5/2}\left(\mu_{b.v} + \frac{4}{3}\mu_{s.v}\right) \int_{-\infty}^{\infty} \frac{1}{\bar{\rho}_i^4}\left(\frac{\mathrm{d}\bar{\rho}_i}{\mathrm{d} z_i}\right)^2 \mathrm{d} z_i, \tag{B48}$$

where the notation "A" is used because this coefficient is the small-ρ_v limit of the regime-1 coefficient A [see formulas (B26) and (B16)].

It remains to transform expression (B48) into its more convenient version (62). This can be done by changing the variable of integration $z_i \to \bar{\rho}_i(z_i)$, where the latter satisfies boundary-value problem (B43)–(B45). Thus, one can deduce that

$$A = \left(\mu_{b.v} + \frac{4}{3}\mu_{s.v}\right) T^{1/2} \rho_v^{-5/2} \int_1^\infty \frac{\sqrt{2(\bar{\rho}_i \ln \bar{\rho}_i + 1 - \bar{\rho}_i)}}{\bar{\rho}_i^4} \mathrm{d}\bar{\rho}_i.$$

Evaluating the integral in the above expression numerically, one obtains (62) as required.

REFERENCES

[1]S. H. Davis, "Contact-line problems in fluid mechanics," J. Appl. Mech. **50**, 977 (1983).
[2]N. Savva and S. Kalliadasis, "Droplet motion on inclined heterogeneous substrates," J. Fluid Mech. **725**, 462 (2013).
[3]J. Eggers and L. M. Pismen, "Nonlocal description of evaporating drops," Phys. Fluids **22**, 112101 (2010).
[4]P. Colinet and A. Rednikov, "On integrable singularities and apparent contact angles within a classical paradigm," Eur. Phys. J. Spec. Top. **197**, 89 (2011).
[5]A. Rednikov and P. Colinet, "Singularity-free description of moving contact lines for volatile liquids," Phys. Rev. E **87**, 010401 (2013).
[6]S. J. S. Morris, "On the contact region of a diffusion-limited evaporating drop: A local analysis," J. Fluid Mech. **739**, 308 (2014).
[7]V. Janeček, F. Doumenc, B. Guerrier, and V. S. Nikolayev, "Can hydrodynamic contact line paradox be solved by evaporation–condensation?," J. Colloid Interface Sci. **460**, 329 (2015).
[8]M. A. Saxton, D. Vella, J. P. Whiteley, and J. M. Oliver, "Kinetic effects regularize the mass-flux singularity at the contact line of a thin evaporating drop," J Eng. Math. **106**, 47 (2017).
[9]A. Y. Rednikov and P. Colinet, "Asymptotic analysis of the contact-line microregion for a perfectly wetting volatile liquid in a pure-vapor atmosphere," Phys. Rev. Fluids **2**, 124006 (2017).
[10]A. Y. Rednikov and P. Colinet, "Contact-line singularities resolved exclusively by the Kelvin effect: Volatile liquids in air," J. Fluid Mech. **858**, 881 (2019).
[11]I. G. G. Barnes, *Interfacial Science: An Introduction* (Oxford University Press, 2011).
[12]E. S. Benilov, "Nonexistence of two-dimensional sessile drops in the diffuse-interface model," Phys. Rev. E **102**, 022802 (2020).
[13]E. S. Benilov, "Can a liquid drop on a substrate be in equilibrium with saturated vapor?," Phys. Rev. E **104**, L032103 (2021).
[14]R. D. Deegan, O. Bakajin, T. F. Dupont, G. Huber, S. R. Nagel, and T. A. Witten, "Contact line deposits in an evaporating drop," Phys. Rev. E **62**, 756 (2000).
[15]G. J. Dunn, S. K. Wilson, B. R. Duffy, S. David, and K. Sefiane, "The strong influence of substrate conductivity on droplet evaporation," J. Fluid Mech. **623**, 329 (2009).
[16]J. M. Stauber, S. K. Wilson, B. R. Duffy, and K. Sefiane, "On the lifetimes of evaporating droplets," J. Fluid Mech. **744**, R2 (2014).
[17]J. M. Stauber, S. K. Wilson, B. R. Duffy, and K. Sefiane, "On the lifetimes of evaporating droplets with related initial and receding contact angles," Phys. Fluids **27**, 122101 (2015).
[18]M. A. Saxton, J. P. Whiteley, D. Vella, and J. M. Oliver, "On thin evaporating drops: When is the d^2-law valid?," J. Fluid Mech. **792**, 134 (2016).
[19]A. W. Wray, B. R. Duffy, and S. K. Wilson, "Competitive evaporation of multiple sessile droplets," J. Fluid Mech. **884**, A45 (2020).
[20]D. J. Korteweg, "Sur la forme que prennent les équations du mouvement des fluides si l'on tient compte des forces capillaires causées par des variations de densité considérables mais continues et sur la théorie de la capillarité dans l'hypothése d'une variation continue de la densité," Arch. Néerl. Sci. Exactes Nat. Ser. **2**(6), 1 (1901).
[21]D. M. Anderson, G. B. McFadden, and A. A. Wheeler, "Diffuse-interface methods in fluid mechanics," Annu. Rev. Fluid Mech. **30**, 139 (1998).
[22]L. M. Pismen and Y. Pomeau, "Disjoining potential and spreading of thin liquid layers in the diffuse-interface model coupled to hydrodynamics," Phys. Rev. E **62**, 2480 (2000).
[23]F. Magaletti, L. Marino, and C. M. Casciola, "Shock wave formation in the collapse of a vapor nanobubble," Phys. Rev. Lett. **114**, 064501 (2015).
[24]F. Magaletti, M. Gallo, L. Marino, and C. M. Casciola, "Shock-induced collapse of a vapor nanobubble near solid boundaries," Int. J. Multiphase Flow **84**, 34 (2016).
[25]M. Gallo, F. Magaletti, and C. M. Casciola, "Thermally activated vapor bubble nucleation: The Landau–Lifshitz–van der Waals approach," Phys. Rev. Fluids **3**, 053604 (2018).
[26]M. Gallo, F. Magaletti, D. Cocco, and C. M. Casciola, "Nucleation and growth dynamics of vapour bubbles," J. Fluid Mech. **883**, A14 (2020).
[27]U. Thiele, S. Madruga, and L. Frastia, "Decomposition driven interface evolution for layers of binary mixtures. I. Model derivation and stratified base states," Phys. Fluids **19**, 122106 (2007).
[28]S. Madruga and U. Thiele, "Decomposition driven interface evolution for layers of binary mixtures. II. Influence of convective transport on linear stability," Phys. Fluids **21**, 062104 (2009).
[29]D. N. Sibley, A. Nold, N. Savva, and S. Kalliadasis, "A comparison of slip, disjoining pressure, and interface formation models for contact line motion through asymptotic analysis of thin two-dimensional droplet spreading," J. Eng. Math. **94**, 19 (2015).
[30]R. Borcia, I. D. Borcia, M. Bestehorn, O. Varlamova, K. Hoefner, and J. Reif, "Drop behavior influenced by the correlation length on noisy surfaces," Langmuir **35**, 928 (2019).
[31]G. Zhu, J. Kou, B. Yao, Y.-S. Wu, J. Yao, and S. Sun, "Thermodynamically consistent modelling of two-phase flows with moving contact line and soluble surfactants," J. Fluid Mech. **879**, 327 (2019).
[32]G. Zhu, J. Kou, J. Yao, A. Li, and S. Sun, "A phase-field moving contact line model with soluble surfactants," J. Comput. Phys. **405**, 109170 (2020).
[33]R. Borcia and M. Bestehorn, "Phase field modeling of nonequilibrium patterns on the surface of a liquid film under lateral oscillations at the substrate," Int. J. Bifurcation Chaos **24**, 1450110 (2014).
[34]M. Bestehorn, D. Sharma, R. Borcia, and S. Amiroudine, "Faraday instability of binary miscible/immiscible fluids with phase field approach," Phys. Rev. Fluids **6**, 064002 (2021).
[35]R. Zanella, G. Tegze, R. L. Tellier, and H. Henry, "Two- and three-dimensional simulations of Rayleigh–Taylor instabilities using a coupled Cahn–Hilliard/Navier–Stokes model," Phys. Fluids **32**, 124115 (2020).
[36]V. Giovangigli, "Kinetic derivation of diffuse-interface fluid models," Phys. Rev. E **102**, 012110 (2020).
[37]V. Giovangigli, "Kinetic derivation of Cahn–Hilliard fluid models," Phys. Rev. E **104**, 054109 (2021).
[38]H. van Beijeren and M. H. Ernst, "The modified Enskog equation," Physica **68**, 437 (1973).
[39]J. W. Cahn and J. E. Hilliard, "Free energy of a nonuniform system. I. Interfacial free energy," J. Chem. Phys. **28**, 258 (1958).
[40]D. Jasnow and J. Viñals, "Coarse-grained description of thermo-capillary flow," Phys. Fluids **8**, 660 (1996).
[41]D. Jacqmin, "Contact-line dynamics of a diffuse fluid interface," J. Fluid Mech. **402**, 57 (2000).
[42]H. Ding and P. D. M. Spelt, "Wetting condition in diffuse interface simulations of contact line motion," Phys. Rev. E **75**, 046708 (2007).
[43]P. Yue, C. Zhou, and J. J. Feng, "Sharp-interface limit of the Cahn–Hilliard model for moving contact lines," J. Fluid Mech. **645**, 279 (2010).
[44]P. Yue and J. J. Feng, "Can diffuse-interface models quantitatively describe moving contact lines?," Eur. Phys. J. Spec. Top. **197**, 37 (2011).
[45]E. S. Benilov, "Dynamics of a drop floating in vapor of the same fluid," Phys. Fluids **34**, 042104 (2022).
[46]E. S. Benilov, "Dynamics of liquid films, as described by the diffuse-interface model," Phys. Fluids **32**, 112103 (2020).
[47]E. S. Benilov, "The dependence of the surface tension and contact angle on the temperature, as described by the diffuse-interface model," Phys. Rev. E **101**, 042803 (2020).
[48]V. Giovangigli and L. Matuszewski, "Mathematical modeling of supercritical multicomponent reactive fluids," Math. Models Methods Appl. Sci. **23**, 2193 (2013).
[49]P. Seppecher, "Moving contact lines in the Cahn–Hilliard theory," Int. J. Eng. Sci. **34**, 977 (1996).
[50]E. S. Benilov, "Asymptotic reductions of the diffuse-interface model, with applications to contact lines in fluids," Phys. Rev. Fluids **5**, 084003 (2020).

[51]J. Kierzenka and L. F. Shampine, "A BVP solver based on residual control and the MATLAB PSE," ACM Trans. Math. Software **27**, 299 (2001).
[52]W. E. Schiesser, *The Numerical Method of Lines: Integration of Partial Differential Equations* (Clarendon Press, Oxford, 1978).
[53]P. J. Lindstrom and W. G. Mallard, see https://webbook.nist.gov/ for NIST Chemistry WebBook.
[54]D. Czernia and B. Szyk, see https://www.omnicalculator.com/physics/air-density for air density calculator.
[55]M. J. Holmes, N. G. Parker, and M. J. W. Povey, "Temperature dependence of bulk viscosity in water using acoustic spectroscopy," J. Phys.: Conf. Ser. **269**, 012011 (2011).
[56]J. Shang, T. Wu, H. Wang, C. Yang, C. Ye, R. Hu, J. Tao, and X. He, "Measurement of temperature-dependent bulk viscosities of nitrogen, oxygen and air from spontaneous Rayleigh–Brillouin scattering," IEEE Access **7**, 136439 (2019).
[57]Z. Brabcova, G. McHale, G. G. Wells, C. V. Brown, and M. I. Newton, "Electric field induced reversible spreading of droplets into films on lubricant impregnated surfaces," Appl. Phys. Lett. **110**, 121603 (2017).
[58]S. S. Sazhin, "Modelling of fuel droplet heating and evaporation: Recent results and unsolved problems," Fuel **196**, 69 (2017).
[59]J. H. Ferziger and H. G. Kaper, *Mathematical Theory of Transport Processes in Gases* (Elsevier, New York, 1972).